FACULDADE DE ENGENHARIA DA UNIVERSIDADE DO PORTO

Human motion reconstruction based on body-worn sensors

Joana Rita Sousa Reis Ferreira da Silva

MASTER'S THESIS

Integrated Master in Bioengineering

Internal Supervisor: João Paulo Vilas-Boas

External Supervisor: Ricardo Matias

October 19, 2018

This thesis had the support of Porto Biomechanics Laboratory, LABIOMEP and Kinetikos team.

LABIOMEP – Porto Biomechanics Laboratory – is a technological center of the University of Porto dedicated to research, innovation and teaching. It studies clinical, sports, engineering and other biomimetic interests.

Kinetikos is a start-up company based in Coimbra, Portugal. Kinetikos instantly translates patient movement into clinical insight to support clinical decision making.

The data from this thesis were collected within LABIOMEP facilities and the post-processing steps at Kinetikos Lisbon's office.

© Joana Rita Sousa Reis Ferreira da Silva, 2018

Ethical Disclaimer

Ethical approval for the studies mentioned in this thesis was granted by the Ethics Committee of Faculty of Sport, University of Porto (Process number: CEFADE 10/2014). All participants were informed about the nature of the studies prior to testing. None of them suffered from any physical impairment.

Resumo

Sistemas ópticos de captura de movimento são ainda recorrentemente utilizados em diversas áreas de reconstrução do movimento, tal como área militar, cinema, realidade virtual e aplicações médicas. Eles recriam o movimento do personagem real num avatar facilitando o seu estudo e/ou projeção em ecrãs virtuais. No entanto, exigem frequentemente um sistema externo complexo, composto por câmaras de infra-vermelho, software específicos e marcadores em pontos relevantes do objecto/corpo. Embora a precisão destes sistemas seja inquestionável, essa dificuldade de portabilidade e o custo elevado associado levou à investigação de alternativas pequenas e móveis, igualmente eficazes mas de manuseamento mais simples. Desta forma, recentemente o uso de sistemas inerciais (IMUs) ganhou grande relevância em diversas áreas da ciência, permitindo avaliar as alterações das propriedades inerciais de um corpo. Eles resultam da combinação de unidades inerciais de acelerómetro e giroscópico que medem respetivamente a aceleração linear e velocidade angular. Surgem em tamanhos reduzidos e sem necessidade de visibilidade, o que expande as suas possibilidades de utilização. Embora as medições de orientação obtidas com IMUs sejam fiáveis, estas tendem a se desviar do valor real quando usadas por longos períodos de tempo. Para colmatar estas falhas surgiram soluções baseadas em algoritmos e no uso de sensores adicionais, tal como o magnetómetro, por vezes incorporado no IMU.

Este projeto investiga a precisão de reconstruir marcha com IMUs colocados nos membros inferiores e pélvis, contra os habitualmente usados sistemas ópticos. Os IMUs utilizados são uma linha sem fios da Xsens, o MTw Awinda, baseados em sistemas microeletromecânicos e incluem acelerómetros, giroscópios e magnetometros de 3 eixos. O sistema óptico é um equipamento da Qualisys, disponível no laboratório de biomecânica da Universidade do Porto. Foram feitos aqui estudos de marcha em sete voluntários saudáveis com os dois sistemas a funcionar a 100 Hz. Os dados recolhidos (ópticos e inerciais) foram convertidos e tratados pelo software proprietário da Kinetikos. Os resultados da comparação entre o sistema ótico e o resultante da Kinetikos são equiparáveis com a literatura. Obtiveram-se entre 2-3°de erro médio absoluto e coeficiente de correlação de Pearson de 0.90 (r).

Este documento contém ainda um estudo preliminar que pretende avaliar o quão promissor é um sistema inercial inovador com dimensões 26.7 x 15 x 4 mm e 2g de massa. Mencionado aqui de Wear, é também um IMU baseado em sistemas microeletromecânicos, e inclui acelerómetro, giroscópio e magnetómetro de 3 eixos. Recorreu-se ainda a uma experiência simples onde os dois sistemas inerciais e o sistema óptico foram gravados simultanemente a 100Hz. O conjunto deslizou repetidamente ao longo de uma calha e foi feita a comparação das acelerações nos três eixos obtendo-se erros médios absolutos inferiores a 1 m/s^2 com r entre 0.91-0.96.

Abstract

Optical tracking systems are still frequently used in several areas of motion reconstruction, such as military, cinema, virtual reality and medical applications. They recreate the movement of the real character in an avatar easing their study and/or projection onto virtual screens. However, these methods often require an extensive external system composed of infrared cameras, specific software and markers at relevant points of the object/body. Although the accuracy of these systems is extreme, the lack of portability and the associated high cost has led to the investigation of small and mobile alternatives, equally effective but simpler to handle. In this way, the use of inertial systems (IMUs) has recently gained great relevance in several areas of science, allowing to evaluate the changes in the inertial properties of a body. They result from the combination of accelerometer and gyroscopic inertial units that respectively measure linear acceleration and angular velocity. They come in small sizes and without the need for visibility, which expands their possibilities of use. Although orientation measurements obtained with IMUs are reliable in the short term, they tend to deviate from the real value when used for long periods of time. To address these shortcomings, solutions have emerged based on algorithms and the use of additional sensors, such as the magnetometer, sometimes incorporated in the IMU.

This project investigates the accuracy of reconstruct human gait with IMUs placed on the lower limbs and pelvis, against commonly used optical systems. The inertial systems used are an Xsens wireless line, the MTw Awinda, consisting of micro-electromechanical systems based IMUs and include 3-axis accelerometer, 3-axis gyroscope and 3-axis magnetometer. The optical system is a Qualysis equipment, available at the Biomechanics Laboratory of the University of Porto. Gait studies were performed here on seven healthy volunteers with both systems operating at 100 Hz. The data (optical and inertial) were converted and treated using a proprietary software, owned by Kinetikos.

This document also contains a small preliminary study that intends to evaluate how promising an innovative inertial system is with dimensions 26.7 x 15 x 4 mm and 2g of mass. Mentioned here as Wear, it is also a micro-electromechanical based IMU including 3-axis accelerometer, 3-axis gyroscope and 3-axis magnetometer. A low-tech methodology was used in which the two inertial systems and the optical system were recorded simultaneously at 100 Hz. The set of systems slid repeatedly along a gutter and it was compared the accelerations of the three axes. The results of the tests with volunteers are comparable with the literature with an absolute mean error about 2-3°and the Pearson correlation coefficient of 0.90 (r). Regarding the sliding test, the absolute mean errors were less than 1 m/s^2 with r between 0.91-0.96.

Ackowledgments

I am glad to express my sincere gratitude to my external supervisor Ricardo Matias, at Kinetikos, and internal supervisor João P. Vilas-Boas in LABIOMEP, for all the fundamental help and guidance in the development of this dissertation. Additionally, I would like to acknowledge this opportunity and for being part of such complete teams and work with high-end technology.

I also want to thank everyone who supported me throughout the development of this work and helped me with the knowledge barriers and integration process. Specially to Jessy Lauer, Márcio Santos, Pedro Fonseca, Sara Morais, and Leandro Machado that provided fundamental insight and expertise that greatly assisted the research. Also, to Champalimaud hardware team, particularly to Artur Silva for his enthusiastic support, as well as to my university teacher, Prof. Diamantino Freitas, for all the availability regarding the preliminary test in this thesis.

To my friends Filipe Marques, Pedro Walgode and Gabriela Samagaio that always encouraged me to keep going and believed in me. Specially to João Costa for the encouragement, exceptional dedication, and for the technical drawings included in this thesis. To my family for all the fundamental support and comprehension, and particularly to my sister and cousin who wisely advised me in problematic situations.

Joana Silva

"The greatest good you can do for another is not just share your riches,
but to reveal to him his own"

- Benjamin Disraeli

Contents

List of Figures

Symbols & Abbreviations

3D	Three Dimensional
ARSs	Anatomical Reference Systems
CF	Complementary Filter
DM	Direct Method
DPE	Direct Pose Estimation
EKF	Extended Kalman Filter
GOM	Global Optimization Method
IHMT	IMU-based human motion tracking
IMUs	Inertial Measurement Units
ISB	International Society of Biomechanics
KF	Kalman Filter
MIMUs or mIMUs	Magnetic Inertial Measurement Units
MoCap	Motion Capture
NESW	North East South West
NOMC	Non-Optical Motion Capture
OMC	Optical Motion Capture
RoM	Range of Motion
SOM	Segmental Optimization Method
UKF	Unscented Kalman Filter
WWW	*World Wide Web*

Chapter 1

Introduction

1.1 Context

There are few things more impacting than life. One of them may be to capture life itself. The human status, the activities we perform, how our connected parts move and how they are not able to move make us an interesting machine of study. Understanding the human movement and its constraints and interactions with the surrounding environment enables the progress in several areas such as health care, sports, robotics, engineering, gaming and cinema. Have you ever wonder how and how much you need to move your arm and eventually standing on your tiptoes to get a glass of water on the shelf? Well, looking at those actions through a perspective of recognizing the mechanics behind them is known as biomechanics [2] and it is quantitatively and qualitatively achieved by instrumenting the movement. Biomechanical insight of the movement without reference to the forces that cause motion entails its kinematic analysis.

One may consider that movement analysis began way back in 1870s with Étienne-Jules Marey and Eadweard Muybridge studying animals and human figure in motion through chronophotography and multiple cameras photographing the movement in a sequence of shots, respectively. However, was in 1915 that Max Fleisher and his 'Rotoscoping' technique made cartoon characters perform like a human, such as Betty Boop. But only later, in 1969 a group of engineers known as Polhemus actually studied human kinematics, using a proprietary electromagnetic motion capture system [3]. Electromagnetic systems use a magnetic transmitter to generate an electromagnetic field and measure sensors' orientation and position relative to that electromagnetic field. Therefore, when nearby metallic instruments they can present considerable error. Also, due to the magnetic field variations within the same room, the capture volume is very small and they require a very careful and frequent magnetic calibration. Latter on, to overcome these magnetic interference, optical marker-based systems have emerged. These lead to very accurate measurements but are confined to a space volume and have marker -occlusion, -detachment and -crossover issues associated. Eager for freedom of movement and natural environment testing, have appeared the professional optical markerless or computer vision based methods. Here the subjects can be studied in real context without all the preparation time, using one single camera, such as Kinect,

to measure a wide range of parameters. However, the 3D reconstruction is computationally demanding and the field of view and depth range may be too short [4]. So, in the latter years Inertial Measurement Units (IMUs) have been largely explored in motion tracking as a free marker alternative which additionally enables applications in uncontrolled environments and more freedom of the movement. These units include on-body gyroscopes, accelerometers, and eventually magnetometers. However, these sensors do not measure position directly and when coupled with magnetometers, may be vulnerable to metal interference. Also, the gyroscope bias (drift) leads to long term instability which may introduce orientation and integration errors in the estimations. Still, when combined with sensor fusion algorithms (a process that combines the three sources of information to improve the estimate of IMU output, e.g. Kalman filters) this can be surpassed. If the accuracy of these systems is proved to be comparable with gold standard approaches, we may witness a huge positive step in motion reconstruction.

Inspired on [5], it was created the comparative Table 1.1 of the aforementioned alternative systems to human motion capture.

Table 1.1: General advantages and disadvantages of most significant motion capture systems inspired on [5].

	Apparatus	Advantages	Disadvantages	Cost
Magnetic	Wearable Exoskeletons;	Portability; Small size	Magnetic and Electrical Interference; Attachment to the body segment of interest; Frequent calibration; Small capture area	$\sim 40€$ (as unit) $\sim 10k€$ (integrated systems)
Optical	Cameras and markers	Wireless; High Accuracy	Multicamera; Occlusion problems; Time-consuming; Interference of light sources; Small capture area	$\sim 130k€$
Computer based	1 Camera	Free movement; No subject preparation required; Natural Environment	3-D structure reconstruction may be computationally demanding and require different software for different applications	$\sim 1000€$
Inertial	Wearable Exoskeletons;	Portability; Small size; Lightweight; Unlimited capture volume	Noise and bias errors; Frequent calibration; Attachment to the body segment of interest	$\sim 40€$ (as unit) $\sim 10k€$ (integrated systems)

As the use of IMUs does not require external cameras or any visibility, they enable more discrete measurements. Also, because these innovative devices are lightweight and cheaper than optical alternatives and continue to be a viable option with relatively accurate results. They are becoming widely marketed (e.g. Xsens Technologies B.V., Synertial and Opal APDM wearable technologies) [6, 7, 8]. Xsens distinguishes itself from the competition because they produce high-end commercial IMUs and are the leading innovator in 3D motion tracking technology [9, 10], even being used as providers of gold standard data [11]. Contrary to optical systems, they also offer out-of-laboratory testing, which is the potential reason why only few studies have examined kicking biomechanics outside the laboratory environment [12].

1.2 Motivation

Regarding the magnetic issues of IMUs some companies such as Xsens (Xsens Technologies B.B, Enschede,The Netherlands) already developed a software that has been validated in magnetically challenging environments. Therefore, these issues can, in one way or another, be eliminated in a wide range of applications. Xsens MVN Analyze Engine is a full-body human measurement system optimized with full magnetic immunity for use in research, sport science, ergonomics and rehabilitation [13]. It is based on inertial sensors, biomechanical models, and sensor fusion algorithms, and can be easily used anywhere.

The usage of IMUs is not restricted as they can be incorporated in a lycra suit (e.g Xsens MVN link) with sixteen inertial sensors connected by wires (Figure 1.1) or using IMU sensors individually and/or through wearable straps like MTw Awinda in Figure 1.2.

In this thesis, we will use the wireless motion tracker version of Xsens: MTw Awinda. It provides 3D angular velocity using rate gyroscopes, 3D linear acceleration using accelerometers and 3D earth magnetic field using magnetometers.

Some applications of the above systems are estimation of spinal loading during manual materials handling and evaluation of amputees walking kinematics (see Figure 1.3) on uneven terrains [15].

Additionally, Inertial Non-Optical Motion Capture technology offers a less intrusive measurement method, being increasingly explored in human performance assessment with application in cinema using virtual characters (see Figure 1.1)

IMUs performance has been matched against to that of optoelectronic tracking systems [10] obtaining encouraging results [8, 9], and even studies with patients with neurodegenerative conditions revealed effectiveness in identifying a range of static physical postures [6]. Although IMUs are small, lightweight and portable, their automated measurements calls for a pre-configuration of the markers and later sensor fusion algorithms implementation (described in section 3.2). Also, the fact they lack of an external visual system, the capture area is smaller compared with optical systems and the sampling rate is below that achieved by the cameras [17].

Several companies invest in developing and selling IMUs and IMU-based systems as Xsens (Xsens Technologies B.B, Enschede,The Netherlands), Invensense (Invensense, San Jose, CA,

Figure 1.1: Xsens MVN Link. The recorded motion capture data is mapped on a digital model in a 3D software which will move like the human actor [14].

Figure 1.2: Xsens MVN Awinda product line. Retrieved from [14].

USA), Trivisio (Trivisio, Trier, Germany) and Microstrain (Lord Microstrain, Willistone, VT, USA). On the other hand, the growing range of IMUs' application also led start-ups to create their own hardware targeting IMU-based systems [10] (see Figure 1.4 for distinct IMU's applications).

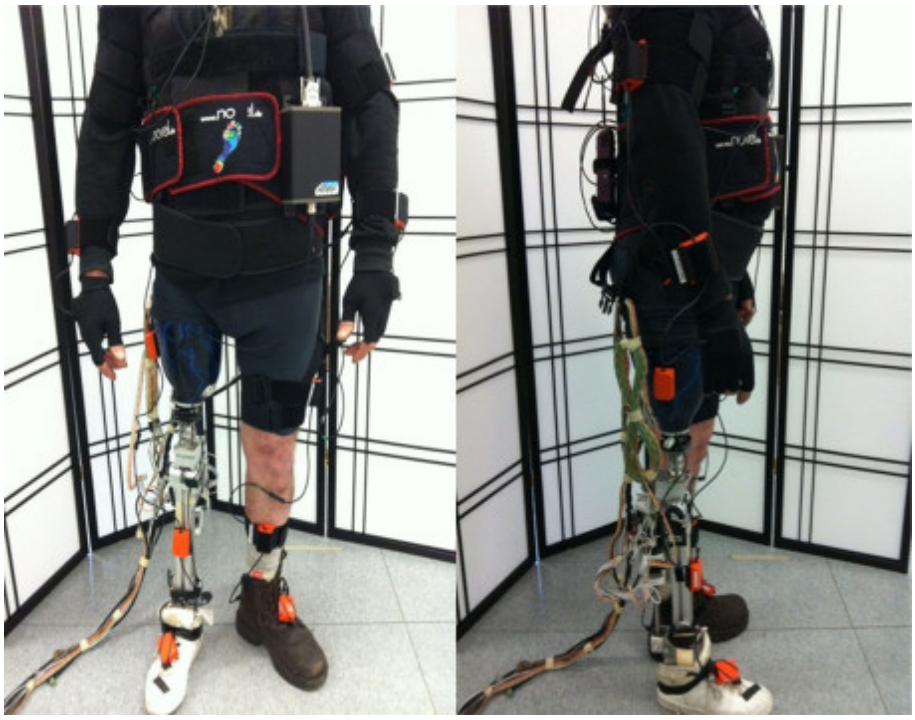

Figure 1.3: Xsens MVN BIOMECH motion capture system where transfemoral amputees walked on uneven terrains with a powered prosthesis [16].

(a) Left bottom: an Xsens MTx IMU. Left top: a Trivisio Colibri Wireless IMU. Right: a Samsung Galaxy S4 mini smartphone.

(b) A Samsung gear VR.

(c) A Wii controller containing an accelerometer and a MotionPlus expansion device containing a gyroscope.

Figure 1.4: Examples of devices containing inertial sensors. Retrieved from [18].

In spite of promising results, the use of inertial sensors has until now failed to demonstrate such a good accuracy like, for instance, OMC systems. Therefore, the motivation for this thesis was to contribute to the body of literature concerning concurrent validity of IMU-based applications in human motion reconstruction.

1.3 Goals

The aim of this dissertation is to assess the accuracy of reconstructing motion with Kinetikos software from multi-planar activities from the daily living based on body-worn inertial sensors. The recordings occurred in Porto Biomechanics Laboratory, LABIOMEP in Porto, Portugal in partnership with Kinetikos team, in Lisboa, Portugal.

For the purpose, derived kinematics from Xsens' IMUs will be compared with Qualisys marker-based system. It is expected to obtain errors between 2° and 3° within the range described in literature [10]. we hypothesize that by combining Kinetikos physics-based models of human biomechanics with measurements of movement from body worn inertial sensors we can achieve an accuracy (+ sensors dynamic accuracy) that equals optical motion-capture data. Additionally, it will be conducted a preliminary test to evaluate the biomechanical potential of a smaller, and still under development, IMU.

1.4 Dissertation Outline

Besides this general introduction, this dissertation contains some background in Human Motion Reconstruction in Chapter 2 and a State of the art on Chapter 3 containing a small review on IMUs' applications, giving relevance on the techniques most commonly used to retrieve and process kinematic data. The Materials and Methods used in the walking trials and preliminary study are described in Chapter 4 and its Results and Discussion are detailed in Chapter 5.

Chapter 6 presents a summary of this dissertation with final remarks, obstacles and future work. Appendix 1 and Appendix 2 provide a review in what concerns the efficiency of non-optical methods in motion tracking studies compared with optoelectronic alternatives and some additional information about the preliminary study.

Chapter 2

Introduction on Human Movement Reconstruction

2.1 Kinematics

Kinematics examines the movement from a spatio-temporal perspective which involves determining how quickly an object is moving or how far it reaches. In other words entails parameters as position, velocity and acceleration of points within the biomechanical system. Therefore, kinematics perceives the movement without considering the causes and effects of the forces involved. For instance, the kinematic analysis of a joint includes determining its angle in relation to a reference system and range of motion (RoM). An example of different kinematic parameters is provided for hip joint in Figure 2.1, where it is described flexion/extension, abduction/adduction and internal/external rotation of the hip.

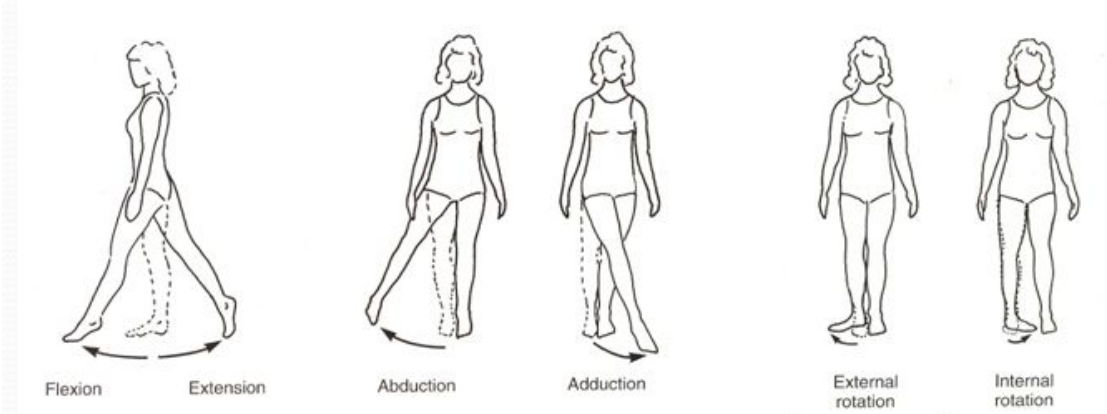

Figure 2.1: Definition of different kinematic parameters for hip joint. Three rotational DoF are presented – flexion/extension (left), abduction/adduction (middle), and external/internal rotation (right). Image retrieved from [19].

To describe a body's position and therefore the position of the human body in space a Cartesian coordinate system is used to define one or more frames of reference [20]. The first frame to be

defined is known as global coordinate system (GCS), which is a laboratory stationary reference fixed in position and orientation and refers to the space volume where the 3D motion is captured. In this project, the GCS is a XYZ right-handed orthogonal system in which the Y-axis corresponds to the principal horizontal direction of motion and X-axis is orthogonal to Y-axis defining the horizontal plane. Z-axis points upward vertically and is perpendicular to XY plane.

However, is still necessary a representation in or within each body segment with reference to that GCS: the relative or local coordinate system (LCS). The definition of that orthogonal frame, also named bone-embedded frame or anatomical frame, entails each bone as a rigid body and defines the relative positioning and orientation of the LCS with respect to the GCS. These were the coordinate systems used in our data, collected at LABIOMEP, and are depicted in Figure 2.2.

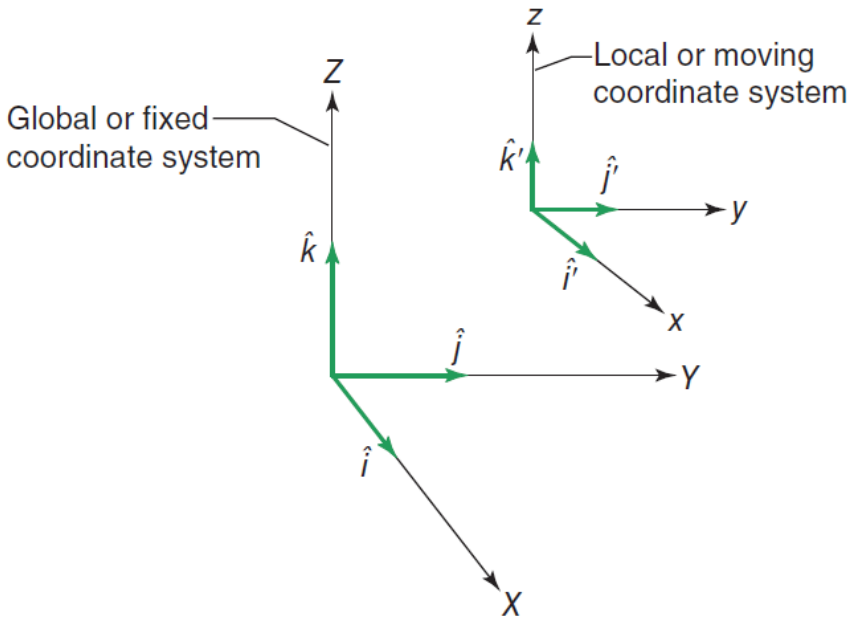

Figure 2.2: The global/fixed and local/moving coordinate systems representations. The unit vectors for the GCS are here termed as $\hat{\mathbf{i}},\hat{\mathbf{j}},\hat{\mathbf{k}}$ and for the LCS as $\hat{\mathbf{i}}',\hat{\mathbf{j}}',\hat{\mathbf{k}}'$ that corresponds, respectively, to the lateral, anterior and superior directions. Image retrieved from [20]

The unit vectors for the GCS are here termed as $\hat{\mathbf{i}},\hat{\mathbf{j}},\hat{\mathbf{k}}$ and for the LCS as $\hat{\mathbf{i}}',\hat{\mathbf{j}}',\hat{\mathbf{k}}'$ (see Figure 2.2). Although in Figure 2.2 both coordinate systems are aligned and rotational transformations are not required, when a rigid segment is moving the different coordinate systems are related by means of a rotation matrix:

$$R = \begin{bmatrix} \hat{\mathbf{i}}'_x & \hat{\mathbf{i}}'_y & \hat{\mathbf{i}}'_z \\ \hat{\mathbf{j}}'_x & \hat{\mathbf{j}}'_y & \hat{\mathbf{j}}'_z \\ \hat{\mathbf{k}}'_x & \hat{\mathbf{k}}'_y & \hat{\mathbf{k}}'_z \end{bmatrix}, \tag{2.1}$$

where R is the rotation matrix from GCS to LCS and $\hat{\mathbf{i}}$',$\hat{\mathbf{j}}$',$\hat{\mathbf{k}}$' are the LCS unit vectors expressed in GCS.

Taking pelvis segment represented in Figure 2.3, the lateral direction $\hat{\mathbf{i}}$' of pelvis' LCS is defined in the GCS by the vector difference:

$$\hat{\mathbf{i}}' = \frac{\overrightarrow{O}_{PELVIS} - \overrightarrow{P}_{RASIS}}{\left|\overrightarrow{O}_{PELVIS} - \overrightarrow{P}_{RASIS}\right|} \tag{2.2}$$

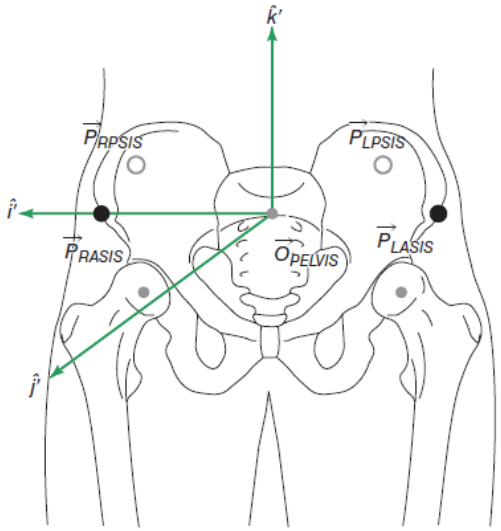

Figure 2.3: The origin of the pelvis LCS ($\overrightarrow{O}_{PELVIS}$) is the central point between the right and left anterior-superior iliac spines: $\overrightarrow{P}_{RASIS}$ and $\overrightarrow{P}_{LASIS}$, that can be used to derive pelvis LCS. Image retrieved from [20].

The vector in the superior direction $\hat{\mathbf{k}}$' is obtained by the cross product between $\hat{\mathbf{i}}$' and an orthogonal unit vector $\hat{\mathbf{v}}$ that connects the midpoint of $\overrightarrow{P}_{RPSIS}$ and $\overrightarrow{P}_{LPSIS}$ to $\overrightarrow{O}_{PELVIS}$:

$$\hat{\mathbf{v}} = \frac{\overrightarrow{O}_{PELVIS} - 0.5 * (\overrightarrow{P}_{RPSIS} + \overrightarrow{P}_{LPSIS})}{\left|\overrightarrow{O}_{PELVIS} - 0.5 * (\overrightarrow{P}_{RPSIS} + \overrightarrow{P}_{LPSIS})\right|} \tag{2.3}$$

$$\hat{\mathbf{k}}' = \hat{\mathbf{i}}' x \hat{\mathbf{v}} \tag{2.4}$$

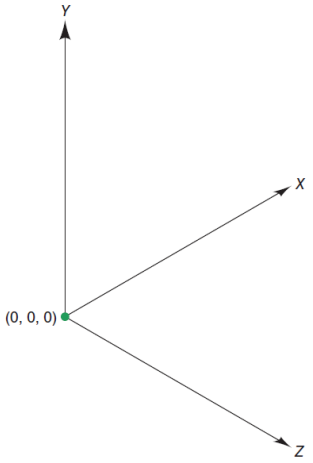

Figure 2.4: ISB's global coordinate system convention.

The anterior vector $\hat{\mathbf{j}}$' is then obtained by the cross product between the lateral direction vector and the unit vector normal to the plane (in the superior direction):

$$\hat{\mathbf{j}}' = \hat{\mathbf{k}}' x\, \hat{\mathbf{i}}' \tag{2.5}$$

Hence, to define the relative bone-orientation in 3D (see Figure 2.4), there are needed at least three angles of rotation, one per axis, known as absolute angles. ISB (International Society of Biomechanics) uses the terms yaw, pitch and roll for rotations (right-handed) about the Y-vertical, Z-lateral and X-anteroposterior axis, in this order. Kinetikos software also uses this representation for the motion reconstruction workflow (see Figure 2.4). These angles are also named in a general way by Euler Angles.

Additionally, the angles between two adjacent bone segments are called relative, joint or cardan angles. Cardan angles, sometimes also grouped with Euler angles differ from the last as for Euler the first and last rotation are about the same axis (for example XYX and YZY). Nonetheless, to fully describe a rigid body we need six independent parameters: the location (X,Y,Z) of it's center of mass and yaw, pitch and roll angles that provide the orientation.

The number of described parameters defines the unique location of the body and is known as the body's degrees of freedom (DoFs). Generally, two anatomical landmarks of the bone define one frame axis and the third point will yield the bone anatomical plane and therefore the other two axis of the frame. Furthermore, its determination should ensure inter- and intra- subject repeatability and requires convenient axis to represent rotations and translations of adjacent joints [21]. Therefore, each frame will be characterized by the bone-associated anatomical landmarks or predicted centers of rotation, which are time-invariant and estimated in the GCS, at each sampled instant of time [22]. These target points will be tracked during the movement by placing markers either into cutaneous (external) or bony (internal) parts. Bone-pin markers comprise invasive approaches and have some ethical concerns and they will not be considered in this dissertation.

Markers are either placed individually or attached to the body within a cluster. When the cluster is rigid it helps compensate relative movements between skin and bone, in the other cases, when using skin markers or non-rigid clusters, algorithms are implemented to compensate for the mentioned artifacts [21]. Nonetheless, the "ideal" position of the markers may be associated with marker-bone displacements [23] or lack of visibility by the cameras. Hence, experimental requirements may triumph against anatomical considerations. More than the three strictly necessary markers per segment may be used to yield a better estimation of bone frame and joint axis.

At sum, kinematics will not account for causes of the biomechanical movement, especially forces and torques [24].

2.2 Inverse Kinematics (IK)

Widespread use of movement analysis, via marker co-ordinates and multi-link models, has been the choice method for reconstruction of the musculoskeletal system motion, with applications in diagnosis, treatment or movement improvement [25]. But does analyzing marker trajectories have clinical significance? Something more meaningful leads to an Inverse Kinematics (IK) problem that requires prior determination of the pose (position and orientation) of the body segment/link. At least three non-collinear markers per segment are needed to specify its reference frame and thus to completely describe its pose. Given a posture configuration, Inverse Kinematics states: "What are the joint variables for that desired position in a desired orientation?". For instance, if someone intends to grab a glass of water, they will not think about how and how much they need to move their wrist, elbow or shoulder. But even to reach the glass there are a few solutions which represent further challenges to solve for the IK problem. However, our biomechanical restrictions prevent many of those solutions from being possible. Explicitly, to calculate lower extremity kinematics using 3D coordinates, we know where the end effector is (in this case the foot) and we want to know what angles in leg segments would be to end up with the end effector in that specific position. Inverse kinematics can still yield different solutions, that may not be naturally attainable by human body, that explains why the joint constrains need to be implemented. It is also possible to use the 3D angle between two vectors but in the case the vectors are not in the same plane this angle does not necessarily represent the desired clinical joint angle. Joints define how the bone segment moves with respect to its parent body, being that the kinematic chain is defined from parent to child joint frame [26]. The preferred method of most motion capture systems is then to calculate the angles based on the local coordinate frames for each segment.

2.2.1 Pose Estimation Algorithms

Biomechanical modelling is frequently used to analyse the motion of a human body. When a body is modeled as series of rigid links, representing each segment, defines a multi-link model. The pose of each segment in a multi-link model can be estimated by different approaches, distinguished by their mathematical complexity and whether or not they cope with biomechanical constraints of the joints and soft tissue artifacts (STA). Joint constraints describe the interactions of a segment with

other segments allowing from zero up to six DoFs. Inverse Kinematics Algorithms may or not compensate for those STA and constrains [27].

The Direct Method (DM)

Direct Methods estimate the LCSs in a dynamic trial in the same manner as they estimate in the standing pose. Direct Pose Estimation (DPE) is the simplest method here described as it does not impose any of those artifacts in the data, and it calculates the segment LCS from two vectors, pointing from one of the three markers to the other two. Having only three markers to compute the LCS and no redundancy to represent the segment means that if a tracking marker is occluded the LCS cannot be defined [20]. Another limitation is that no kinematic constraints are considered between adjacent bones and all six DoFs are attained [27, 21].

Segmental Optimization Method (SOM)

Generally, STA can not be avoided unless one uses bone-pin markers. As so, in attempt to reduce their influence, Segmental Optimization Method (SOM) appeared, which estimates the segment pose minimizing the errors between the virtual model and the experimentally placed markers. The segment pose is achieved by a transformation matrix in a least-squares sense but it does allow for non-anatomical joint displacements [27]. On the other hand, Global Optimization Methods (GOM) do not treat each segment independently and apply joint constraints for the entire limb or body preventing apparent joint dislocations, giving more reliable values for joint kinematics.

Global Optimization Method (GOM)

As now intensively used (e.g. in Kinetikos software), the GOM formulation, which additionally has the asset of considering internal coordinates to map complex smooth and continuous joint motion, known as "mobilizers". Mobilizers can be thought as the mathematical reverse of joint constraints. While a constraint removes DoFs from a model, a mobilizer grants DoFs to a body [28]. These are particularly useful in modeling biomechanics because coordinates became directly related to the DoF of interest [29]. Joint frames orientation as reported in this thesis was computed according ISB recommendations. Kinetikos software will be used to model participants as a multi-link chain where body segments are represented as rigid links, and to further perform data analysis.

2.3 Ways to Human Movement Reconstruction

Capturing the three-dimensional (3D) human motion and transfer it to a digital model can be attained either by optical or non-optical systems. Optical systems use tracking cameras (with or

without markers), while the systems that measure inertia or mechanical motion are referred to as non-optical. Currently, the standard choice for biomechanical monitoring are the optical motion capture systems [30], justified by their high resolution measurements and extreme accuracy in reproducing the precise position in virtual environments. Nonetheless, these systems are quite constrained to experiments in a controlled environment and so the lack of portability and capability to collect real-world data led to the adoption of wearable systems as inertial measurement units (IMUs). IMU-based human motion tracking (IHMT) systems are also easier to use, have a shorter setup routine and provide instant validated data output.

2.3.1 Optical Motion Capture (OMC) Systems

Optical image-based sensing systems generally reconstruct the participant's posture by using multiple cameras that track predetermined points, usually specific bony landmarks [5]. Optical as the term suggests, means related to sight, involving some visual tool to capture the motion. It can be simply visible light, used on video-based systems or infrared-based devices. As a result, they may require infrared (IR) emission cameras and reflective markers or pulse infrared light emitting diodes (LEDs) attached to the segments of interest. OMC systems have an integrated software, call for a calibration wand and may be coupled with force platforms when measuring specific parameters of locomotion (see Figure 2.5 for a general example).

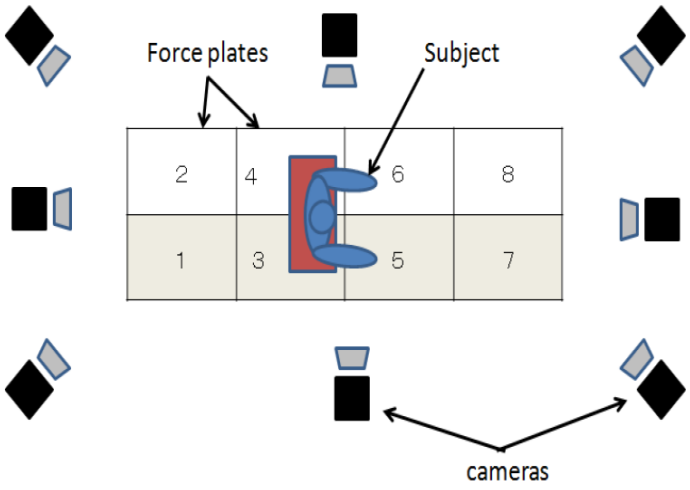

Figure 2.5: Motion capture system adopted in [1].

Examples of the most commonly used tracking systems are Vicon and Qualisys motion systems. Here, full body kinematics assessment needs between eight and sixteen (sometimes much more) high-quality cameras, and only one or two cameras for facial motion recognition [17]. Optical systems can be further segmented into passive - if the infrared cameras track the retro reflective markers and active - when the motion is captured through the emission of light from LED markers.

Optical-passive methods comprise reflective markers, usually rubbers coated with retro-reflective material, that reflects the incoming IR light back to the cameras. Spherical markers are the most common choice as they reflect the light at each possible angle with respect to the tracking system [31]. Optical-active approaches are less handy as they need wires to connect the LEDs or battery to operate and emit IR light. Nonetheless, as they do not depend on reflecting IR light from the cameras, the tracking distance can be increased and thus, a greater volume measurement is attained. These approaches have the disadvantages that the emitted or reflected light might be blocked during the movements, and therefore the resulting kinematic representation would be adulterated in relation to real-world data. Moreover, the markers may also detach or move from the original position and for these reasons the motion capture needs to be in a controlled environment.

Furthermore, literature reports that joint kinematics and segment pose reconstruction from marker-based studies are harmed by the presence of soft tissue artifacts. STA are the most intractable cause of inaccuracies when measuring the underlying bone movements. They are translated into skin movements, muscle contractions and wobbling masses and can lead to rigid motion (rotations and translations) and/or non-rigid motion (deformation) of the measurement clusters [23]. Hence, the optimal limb region to place the cluster will be the one with the least movement artifacts, avoiding bony prominences, for instance. To further minimize the error propagation in kinematic reconstruction, a minimum of four marker-cluster is needed to extract the rigid motion component and its longest principal axis should be orientated and aligned with the anatomical landmarks [22]. Moreover, STA distribution maps for the tight and shanks located the minimum STA on the lateral side of the lower half of the limbs [23].

To scale a lower limbs biomechanical model, one should register Body Measurements of each participant such as, body mass and height, shoe size, hip height, knee height, ankle height and hip width [32]:

(i) **Foot size** — Is measured from the back of the heel to the front of the toe;

(ii) **Arms' span** — Measured fingertip to fingertip;

(iii) **Ankle height** — Is measured from the floor to the center of the ankle;

(iv) **Hip height** — Is measured from the floor to the greater trochanter. Additionally the anterior superior iliac spine (ASIS) should be measured for hip width. Usually coincides with the center of the leg;

(v) **Knee height** — Is measured from the floor to the lateral epicondyle. It can be found by locating the space between the lower and upper leg and moving slightly upwards;

(vi) **Shoulder width** — Is the distance between the left and right acromion;

(vii) **Shoulder height** — Is the distance between the floor and the left or right acromion.

Many platforms are available to treat MoCap data, such as, Anybody, Visual 3D and OpenSim. In this thesis Kinetikos software was used to reconstruct motion from either Qualysis and Xsens data sources.

Biomechanical in vivo studies like this, that intend to attain the most correct interpretations of the movement might require medical imaging tools to precisely estimate the center of rotation of the involved joints [33]. However, when equipment are unavailable, the joint centers (for example, the shoulder complex, hip and knee) may be estimated via functional movements and mathematical approaches. Before proceeding with any simulation, the marker data can be filtered in order to attain a cleaner motion. The data from the optical system might then be low-pass filtered using a fourth-order Butterworth filter with zero-lag and a cut-of frequency of 10Hz [34] using Vicon 3D, Matlab [35] as well as other programming languages [36].

2.3.2 Motion Reconstruction Workflow

Data collected either with Qualysis motion system and Xsens IMUs was used to reconstruct subjects motion through Kinetikos pipeline constituted of Scaling, Posing and IK.

2.3.2.1 Scaling and Model Posing

The Scale tool is meant to adapt the chosen model dimensions and weight to a specific subject. The final dimensions of the generic model are accomplished via scale factors automatic computation. The scale factors can be set manually or calculated based on the distance between analogous marker pairs in the model and the subject. For example, if the virtual distance between pair 1 is **m1** and the correspondent experimental distance for the same pair is **e1** the scale factor being applied to the body segment containing this markers will be $\mathbf{s1}=\frac{\mathbf{e1}}{\mathbf{m1}}$.This is then applied uniformly to all segments or the user can select which markers' distances will be used to scale which segments

Relative weights can be assigned to each of the selected markers. These weights determine to what degree the algorithm should try to match them, concerning to others. For example, if the RASIS (Right Anterior Superior Iliac Spine) marker has a weight of 10 and RKNE (Right Knee) marker a weight of 1, the first will be ten times more tightly tracked than the last, and the tracking errors will also be more penalized. Thus, generally, the markers weighted more heavily should be the ones that more closely match the experimental, like those placed on bony parts, which are less likely to be misplaced. Regarding the segments' mass adjustments, two approaches can be used: (i) The first one preserves the mass distribution, i.e, guarantees that the segments in subject's specific model are scaled in the same proportion as they were in the generic model. This way, the scale factor applied to each segment will be independent from the ones determined for scaling the segments' size and the final total mass will correspond to the subject's. (ii) The second approach blindly applies the scale factors computed for the size scaling also for the mass adjustments and so, will presumably not correspond to the total mass of the subject.

Scaling is an important step in accurate human motion reconstruction. We strongly advise to preview how the scale segments and corresponding markers march the experimental ones.

Once scaling is achieved model's joint generalized coordinates are modified in such a way that the model match as accurate as possible the experimental pose (e.g. first frames of data collection) just like an IK problem. This can be achieve in the Kinetikos software either by manually entering

model's generalized coordinates values (if known) or by using the Kinetikos Posing tool which asks for a set of distances between specific bony landmarks that can be directly measured using a tape.

2.3.2.2 Inverse Kinematics

In Kinetikos software (like in many others) the IK tool reconstructs subject's motion by varying the kinematic model joint angles (generalized coordinates) in such a way that: (i) the model markers will track (and try to minimize the distance to) the experimental ones in each time step (frame) in the case of using 3D markers coordinates; (ii) the model segments' orientation will track the given IMUs Euler rotations given by the sequence XYZ. In both cases, the IK tool solves a weighted least squares problem that aims to minimize marker's/Euler angles and unprescribed coordinate's error term. Unprescribed coordinates are those calculated using IK that are unlocked and whose trajectory is unknown, contrary to prescribed coordinates whose value is reliable enough to remain unchanged and so they are not used in IK solver.

$$min_q \left[\sum_{i \varepsilon markers} w_i \left\| x_i^{exp} - x_i(q) \right\|^2 + \sum_{j \varepsilon unprescribed\ coords} \omega_i \left(q_j^{exp} - q_j \right)^2 \right]$$

$$\mathrm{q}_j^{exp} = q_j, for\ all\ prescribed\ coordinates\ j \quad (2.6)$$

where, having as an example the marker-based solution, $\mathbf{q}$ is the computed vector of generalized coordinates, $\mathbf{x_i^{exp}}$ the experimental position of marker $\mathbf{i}$, $\mathbf{x_i}(\mathbf{q})$ the corresponding position on the model and $\mathbf{q_j^{exp}}$ the experimental value for the coordinate. The time range in which the IK will be performed is user-specified, depending on the study goal. If not specified it will run the entire frames of the trial.

Such a solution is also used by Kinetikos to reconstruct subjects motion in real time as seen in Kinetikos biofeedback tool.

2.3.3 Non-optical Motion Capture Systems (NOMC)

Although traditional optical systems allow for extremely faithful motion reconstruction in most cases, they are limited to the laboratory workspace that the experiments are confined. Added to their complexity, those systems are operationally intensive and comprise an expensive hardware. Non-optical alternatives emerged in motion tracking research to overcome those limitations, offering a small size and automatic data capture from areas where visibility is impaired or impossible [6] without the need of external cameras. These technologies include inertial and electromagnetic systems [17] and they may combine different types of sensors: gyroscopes, accelerometers and magnetometers, as can be depicted in Figure 2.6.

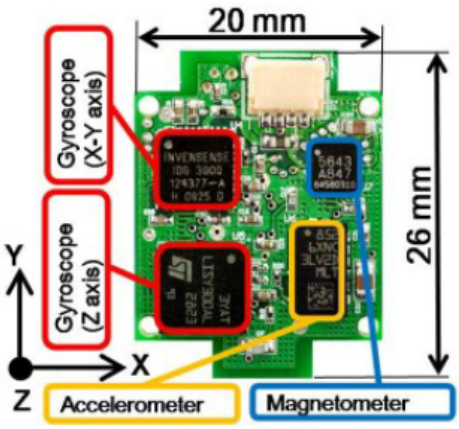

Figure 2.6: Waseda bioinstrumentation system No.3 (WB-3) IMUs presented in [1].

2.3.3.1 Inertial Motion Tracking Sensors

Kinematic applications paved the way for the use of wearable sensors as inertial NOMC systems, referred to as IMUs. They result from a combination of inertial measurement units of accelerometer, gyroscope and magnetometer (see Figure 2.6) that can either be incorporated on a suit or used individually discarding the need for visibility.

These three sensors are useful for determining position and orientation, but they measure different quantities.

The accelerometer measures the kinematic variable of acceleration which can be integrated once to measure changes in velocity and integrated twice to measure changes in position. An accelerometer at rest provides a straight upwards reference which is the linear gravitational acceleration.As a result, tilting the accelerometer up and down it will vary between $\pm$ 1G ($\approx \pm 9.81 m/s^2$). However, during dynamic conditions the accelerometer's output does not distinguish the gravitational acceleration from the external acceleration of the object/body is attached to. Meaning that the gravity component with respect to the sensor frame changes according to the modifications in the sensor orientation [37].

The gyroscope measures either changes in orientation (regular gyro) or changes in angular velocity (rate gyro) reacting quickly to this changes, unlike the accelerometer, however, it accumulates enormous error over time.

A magnetometer is a sensor that measures the local magnetic flux density which is directly proportional to the magnetic field strength. Therefore, a magnetometer senses magnetic fields, namely the Earth's magnetic field. Hence, without worrying about how it is held the magnetometer can be used as a compass to guide us in the NESW (North East South West) plane.

Therefore, if we combine accelerometer and gyroscope signals it would provide an accurate and quick measurement of tilt and orientation concerning gravity (referred to as roll and pitch angles). Nonetheless, the orientation is typically calculated by integrating the angular velocity from gyroscopes, which originates a small drift that leads to an increasing integration error over time. In

other words, the longer the inertial system is used, the higher the drift on tracking points' velocity, making the estimation no longer reliable [38, 10]. Still, accelerometer and gyros data would lack information on sensor's orientation about vertical direction (heading or yaw angle) [39].

The magnetometer senses the magnetic North and corrects sensor's vertical reference solving this drift drawback and calculate yaw. Thus, researchers combined accelerometer and gyroscopes sensors with magnetometers to yield what is known as Inertial Measurement Unit (IMU). Even if the unit is not purely inertial as soon as magnetometers are added. The magnetometer is then used as an earth-fixed reference for the current estimation of the IMU orientation [10], before the gyroscope data is integrated.

For those reasons, such three-sensor combination will enable the monitoring of the rotational velocity of a body in relation to the earth [40] given by Roll, Pitch and Yaw measurements, seen in Figure 2.7. These components will yield the full 3D geometric position of the link (body segment) through its X,Y and Z coordinates, respectively. In this case, when they contain 3-axis accelerometers, 3-axis gyroscopes and 3-axis magnetometers, they may also be recognized as Magnetic Inertial Measurement Units (MIMUs) [41], mIMUs or IMMUs [10, 42]. In this dissertation we will use two IMUs following those specifications: Xsens and Wear.

Together, these sensors allow for quick and accurate 3D position and orientation determination with a low amount of drift over time.

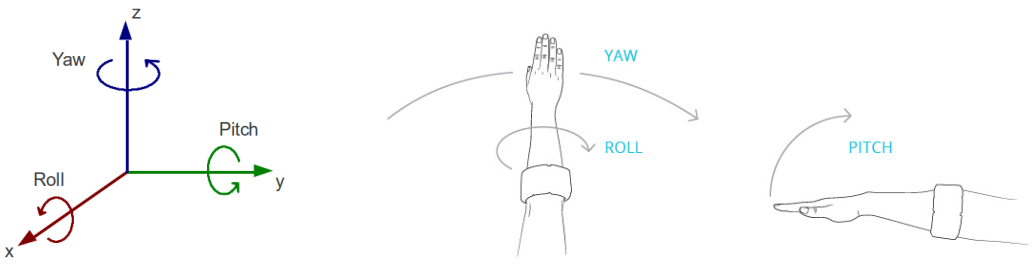

Figure 2.7: Roll, Pitch and Yaw representation in a reference coordinate system (left) and in a shoulder movement example (right), retrieved from [43].

Chapter 3

State of the art

In this chapter are briefly described ways that IMUs are currently incorporated to reconstruct human movement and how they are compared with the gold standard optoelectronic systems accuracy. First is given an overview of the existing comparison studies that match this dissertation goals: daily living activities, namely lower limbs' and gait assessment studies. These are the focus of this project, but other applications where IMUs are already considered an alternative system to optoelectronic ones are also presented in the end of section 3.1. To attain that goal, it was carried out a literature survey on Scopus and Web of Science databases with keywords as: [IMUs OR Inertial (as Title or Abstract)] AND [[Cameras OR Optical OR Vicon OR Qualysis] OR Kinematics (as Title or Abstract)] In section 3.2 are explored in more detail the methodological approaches going throughout the data analysis and processing strategies.

3.1 Literature Review

With the growing need to track human movement in outside environments, emerged the use of inertial systems for its simplicity, discretion and portability. IMUs have become popular in wearable human motion tracking as they are compact devices and can be easily integrated in inertial measurements of different daily activities. Several studies have incorporated IMUs to reconstruct kinematic parameters of human movement and evaluate its accuracy towards the standard optical methods of Motion Capture (MoCap). These methods may differ in the IMU itself, as these may comprise accelerometers and gyroscopes or also magnetometers, and in the data filtering steps. The methods can also be distinguished by the type of optical motion capture system they use and whether they are passive or not [17]. Some of IMUs applications are on sports field, where their small size is particular attractive for outdoor measurements.

3.1.1 Daily living activities

The effectiveness of these inertial systems was proved in sit-to-stand experiments, conducted to aid elderly people [44]. Vicon Optical Motion Capture (OMC) system was used and two IMUs were placed on the leg and trunk of the patient. The data retrieved from the inertial sensors was fused

through an Adaptive Neuro-Fuzzy Inference System (ANFIS). Both resulting outputs would drive an assistive system, including a robot arm and an active walker to imitate a caregiver's motion during supporting tasks (see Figure 3.1). The path generated with IMUs accurately reflected the one estimated with Vicon with a max error of 0.04 m.

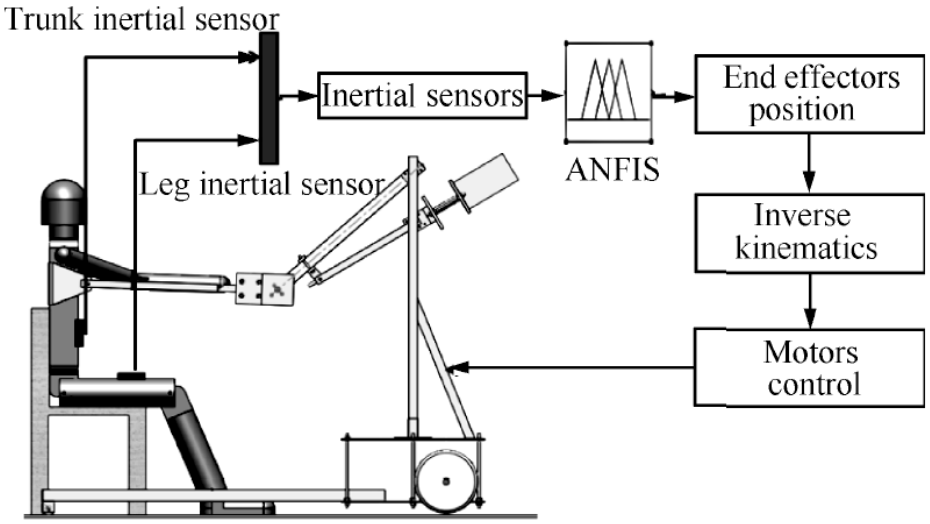

Figure 3.1: Diagram of the interactive control between patient and the assistive device proposed by Salah et al. [44]. The posture of the patient is reconstructed by two IMUs placed on his trunk and leg. The reference for the end effector in world coordinates is generated by ANFIS algorithm and the joint variables are determined through inverse kinematics to drive the device.

Later on, the same author [1] achieved great results using the same ANFIS method in sit-to-stand experiments to estimate the position of the shoulder. He also proposed the ANFIS followed by a Kalman Filter (KF) to reduce the mismatch between sequential measurements. With and without the additional KF step the max match error was 0.06 m and 0.035 m for the x direction and approximately 0.05 m and 0.04 m for the y direction. In these experiments the participants have one IMU placed on the trunk and other on the tight, and are asked to sit with their arms on the chest.

Strong results at lower limbs were obtained with a single IMU placed on lower back during a planar squat task [45]: RMSD estimation in knee joint kinematics about 2.0 ± 1 degrees, in hip joint 3.1 ± 0.9 degrees and ankle joint 3.2 ± 1.0 degrees with average correlation coefficients greater than 0.9. The IMU data was processed with a WFLC (Weighted Frequency Fourier Linear Combiner) filter to find the best estimation of its position and orientation. The algorithms were validated on a humanoid robot (twenty-one DoFs) and eight healthy human volunteers and compared with nine-camera stereophotogrammetric system (MX, Vicon).

Joint kinematics was estimated in underwater flykick [46] through four 9-axis IMUs (with accelerometer, gyroscope and magnetometer) and a rotary encoder being compared with manual digitization. The data from each IMU was processed with an EKF and AnyBody was used to create two musculoskeletal models. The joint angles estimated through inverse kinematics (and the

muscle activities simulated through inverse dynamics) agreed closely for both manually digitized and the IMU driven simulations. Knee flexion had the lowest normalised root-mean-square error (NRMSE): 0.12 and the highest coefficient of determination (R^2): 0.94. The worst NRMSE was obtained in pelvis-thorax flexion: 0.37 and the worst R^2 in hip flexion: 0.43.

In 2011, a contrasting approach described in [47] continuously tracks shoulder and elbow angles with two inertial sensors placed near the wrist and on the upper arm, between the shoulder and elbow, and validates the method with a Vicon optical motion tracking system. The angles are estimated using the Unscented Kalman Filter (UKF) and the algorithms can be generalized to track any limb movement, in either real-time or off-line, with higher accuracy for slow and fast motion with a minimal number of sensors. It obtained a correlation between the two approaches higher than 0.90.

Focused on upper limbs kinematics, [10] compares five non-optical different methods with Vicon OMC system to reconstruct a human arm motion. All the techniques resort to IMUs but they differ essentially on the sensor fusion algorithm choice, using Complementary Filters (CF) and variations of KF, on whether or not they incorporate magnetometer signals, and one of them exploits an additional visual reference for tracking the upper limbs. These methods also differ concerning the kinematic models, some use the Denavit–Hartenberg (DH) convention, others use Euler angles and some use quaternions. Error and correlation were evaluated in each method: elbow flexion-extension ranged between 38.8 and 89.2 mm | 0.77 and 0.91, for shoulder flexion-extension ranged between 82.7 and 214.4 mm | 0.49 and 0.89, and shoulder abduction-adduction between 66.0 and 272.2 mm | 0.36 and 0.73. Regarding the correlation between the real movement pattern and estimated position, one of the methods that performed better resorted to the additional visual reference to estimate trunk orientation and the wrist position, and Extended Kalman Filter (EKF) to provide shoulder and elbow angles. The other best performing method developed a seven DoFs hierarchical kinematic model of each arm according to DH approach, and adopted UKF as sensor fusion technique.

3.1.2 Sport

In football-related activities, IMUs demonstrated good agreement with OMC in quantifying lower extremity kinematics during walking (RMSE: Picerno et al., 2008, 0.8-3.6; Zhang et al., 2013, 1.8-2.4) and running (RMSE: Cooper et al., 2009, 0.7-3.4; Ferrari et al., 2010, 0.6-5.0) [12]. Five reflective markers were attached on a golf club and Vicon MX20+ motion tracking system with eight 2.0 megapixel cameras were used to compare position and orientation estimated of a golf club in space. The study used a Memsense Nano IMU with merely accelerometer and gyroscope data. High-fidelity validation during golf swings was not achieved concerning golf club position [35] but presented almost perfect match regarding golf club orientation in space. The IMUs performance was also validated in robotic motions, using raw data wearable IMUs by APDM [7] and eight-camera Vicon motion-tracking system with passive retro-reflective markers.

Nonetheless, validation with robots provides programmed and repeatable movements i.e, without major issues or external influences to question the reliability of the results.

3.1.3 Clinical Assessment with IMUs

Recently, the strengths of IMUs were also exploited to detect walking disorders in patients with parkinson's disease, with and without turning episodes [8]. The steps were detected with an algorithm developed on the basis of a continuous wavelet transform (cwt) and the data were extracted from a single 6-axis IMU (ADPM) at the lower back. The heel strike and toe off time detection were compared with a Vicon optoelectronic system and the results demonstrated accuracies greater than 0.88 for both episodes being that the results for non-turning episodes were slightly better, reaching 0.91. Currently, regarding step detection, the potential of IMUs gave rise to a wearable low-cost sensing system [9] that along with ultrasound sensors and a particle filter was capable to provide tracking errors less than 2%. A modified version of EKF used two update measurements from two proximity sensors to correct the estimated position and the validation of the system was provided by a Vicon motion capture system.

It can be perceived that wearable devices applications are able to cover different health care areas such as gait analysis, stabilometry, instrumented clinical tests, upper-body mobility assessment, daily-living activity monitoring and tremor assessment (see summary table of IHMT methods in [10]). Yet, each of these applications implies distinct methodologies, depending on the experiment, or the body part kinematics one intents to assess. For instance, concerning the upper limbs and spine kinematics, the clinical application of inertial systems is still little explored being that optical systems are typically chosen. Even so, some simple approaches carried out experiments using one single IMU placed on the upper arm. However, they revealed that the level of detail provided by one IMU is insufficient and amplifies the compensatory strategies' interference that occur in the trunk [39]. On the other hand, for sit-to-stand tests, a single sensor positioned on trunk of the subject is enough to obtain feasible kinematic information in patients with Parkinson's disease [48]. Stabilometry tests focus on analyzing the parameters collected about the center of pressure on foot which are properly and directly provided by stabilometric and barodopometric platforms what does not justify the purchase of IMUs [39].

3.2 Processing of IMUs data

Data processing steps are crucial to have meaningful motion capture data, and include aligning the orientation of the involved reference coordinate systems and possibly some data denoising and drift elimination. There are two main reference systems of interest:

(i) Laboratory reference frame — The optoelectronic system reports data in this frame and the IMU data will be converted into this frame.

(ii) Subjects' reference frame — This frame moves during the movement of each body segment and it is stationary with respect to the corresponding IMU.

Estimating a body's position and orientation goes through determine the kinematic equation for a specific rotation of the body [10] :

$$\dot{R} = RS(\omega) \quad with \quad S(\omega) = \begin{bmatrix} 0 & -\omega_z & \omega_y \\ \omega_z & 0 & -\omega_x \\ -\omega_y & \omega_x & 0 \end{bmatrix}, \tag{3.1}$$

where S(ω) is the skew-symmetric matrix of vector ω, the angular velocity or rotation rate vector of the body-fixed coordinate system. The rotation R represents the orientation of the body-fixed reference frame related to earth's reference frame.

However, Equation 3.1 is susceptible to numerical errors that continuously grow when applied to sensors that drift with time. Like this, with gyroscopes or accelerometers that suffer from time varying biases and noises, R will stop representing a rotation, at some point [10]. For this reason, researchers started exploiting both algorithmic and hardware strategies as ultrasonic sensors, GPS, ultra wide bands (UWB), cameras, and magnetic field generated by actuated coils, to solve the drift issue [10]. Even so, the non-linearity of Equation 3.1 harms the implementation of filtering algorithms as it is described in section 3.2.

Additionally, there are few other ways to represent the rotation that influence the choice of the filtering algorithm. Most well-known are the representations by a rotation matrix, Euler angles and quaternions, each one having its own set of advantages and disadvantages [49].

Seaman et al. [35] suggested that the rotation cited above may be attained by quaternions or Euler angles.

A quaternion is a four-dimensional complex number that can also represent the orientation of a rigid body in the three-dimensional space:

$$\overset{A}{B}\mathrm{q} = [q_1\ q_2\ q_3\ q_4] = [cos\tfrac{\Theta}{2}\ -r_x sin\tfrac{\Theta}{2}\ -r_y sin\tfrac{\Theta}{2}\ -r_z sin\tfrac{\Theta}{2}], \tag{3.2}$$

where $\overset{A}{B}q$ describes the orientation of frame B relative to frame A and ${}^{A}r$ is a vector described in frame A. r_x, r_y and r_z define the components of the unit vector ${}^{A}r$ in the x, y and z axis of frame A, respectively.

Since any rotation of a body around a direction gives the same vector but a different quaternion, the problem is solved by converting the measured acceleration vector into a quaternion [50]. A graphical visualization of a quaternion is in Figure 3.2 .

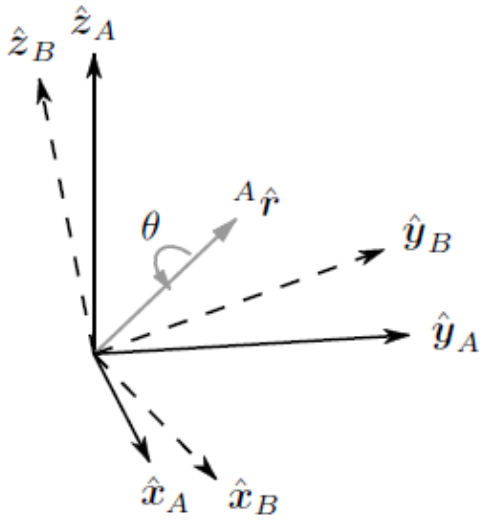

Figure 3.2: Quaternion representation. The orientation of frame B is achieved by a rotation, from alignment with frame A, of angle θ around the axis ^{A}r. Retrieved from [51].

Different software can be used to treat the data from Xsens. For example, MVN Studio BIOMECH, now called Xsens MVN Analyze [52], which simultaneously gives a real-time preview on screen and records the data and Visual3D, a generic biomechanical software that allows to collect further information about movement. MVN Analyse is a full-body human measurement system based on inertial sensors, biomechanical models, and sensor fusion algorithms. Easy to use with short setup time and instant validated data output. Once the data is collected (e.g. Xsens), it can be automatically pushed into Kinetikos online platform where proprietary biomechanics models reconstruct the motion and output in real time calculated joint angles.

Accelerometers, gyroscopes and magnetometers units, contained in the IMU, create data that needs further sensor fusion techniques to obtain useful information about the limbs' position and orientation. Some of these techniques are detailed below, being that the one here used to output Euler Angles is implemented by Xsens, a Kalman Filter (KF) - based technique.

3.2.1 Sensor Fusion algorithms

Inertial systems alone have poor stability and are very sensitive to errors in the rotation rates and accelerations, as mentioned in section 1.1. To overcome these problems the data retrieved from the different inertial units within an IMU can be fused differently. This is attained through sensor fusion techniques that are implemented with the aim to provide feasible orientation and position information. Sensor fusion algorithms determine the heading, pitch and roll (mentioned in Chapter 2) from the outputs of motion tracking devices. Several algorithms can be used to attain these measures, being that, the three most common approaches are: (i) Complementary Filter (CF) and (ii) Kalman Filter (KF):

(i) **Complementary filters** are applicable to IMUs consisting of 3-axis gyroscopes and 3-axis accelerometers, and magnetic angular rate and gravity (MARG) sensor arrays, that also include 3-axis magnetometers (six DoF and nine DoF sensors, respectively) [53]. Hence, CF are able to fuse either data from 6-axis IMUs or 9-axis IMUs. Madgwick filter is the most common example, and uses a quaternion to represent a body's attitude in order to eliminate the ambiguity when the direction is determined with a vector.

The algorithm performance is further controlled by an adjustable parameter, β, that compensates the drift from gyroscope (explained in 2.3.3), and represents the trade-off between accuracy and response speed [36]. This filter also includes an analytically derived and optimized gradient descent algorithm enabling performance at low sampling rates; an on-line magnetic distortion compensation algorithm; and gyroscope bias drift compensation [51]. Mangia et al. [54] used this Madgwick filtering to estimate the attitude and pose of the bodies in water environment, applied to 9-axis IMUs. The filter is relatively simple and computationally light, being perfect for small embedded systems [55]. Another complementary filter, suggested by Mahony et al., also employs quaternion representation for orientation estimation applicable to IMUs, offering efficient performance with little computational cost [56].

(ii) **Kalman Filter (KF)**, along with its variants (as Extended KF (EKF), and Unscented KF (UKF)) are the most widespread sensor fusion technique. They accurately estimate the desired orientation and reconstruct the 3D position of the segment in which the IMU is placed [10]. Although they are very powerful, they are a lot more complex than complementary filters, due to its hard-understanding Gaussian probability density functions (pdfs). EKF approach is a manipulation of KF, generally adopted when dealing with nonlinear equations [10]. UKF are used to provide even more accurate estimation of the pdfs under nonlinear transformations.
The success of KF is due to its small computational requirement, elegant recursive properties, and its status as the optimal estimator for one-dimensional linear systems with Gaussian error statistics [57]. The Kalman Filter model assumes that the state of a system at a time, *t*, evolved from the prior state, at time *t-1*, according to the equation [57]:

$$x_t = F_t x_{t-1} + B_t u_t + w_t, \tag{3.3}$$

where x_t is the state vector that contains the position, velocity or heading at time t, u_t is the vector containing any control inputs. F_t is the state transition matrix, which applies the effect of each system state parameter at time *t-1* on the system state at time t (position and velocity at time *t-1* affect the position at time t). B_t is the control input matrix, which applies the effect of each control input parameter in the vector u_t on the state vector. w_t is the vector containing the process noise terms for each parameter in the state vector via

covariance matrices. The KF further involves a prediction and measurement update stages (additional information about KF implementation can be found in [57]).

Salah et al. [1] adopted KF for sit to stand experiments and Seaman et al. used EKF applied to golf swings in [35]. Zizzo et al. in [9] included a modified version of EKF, that provides periodic corrections for the algorithm during human walking motion.

Chapter 4

Materials and Methods

In this study we conduct a concurrent validity study where we validate an IMU-based motion reconstruct system, the MTw Awinda (Xsens Technologies B.V., Enschede, the Netherlands) versus a 12 camera optical motion capture system (Qualisys AB, Sweden). Seven healthy subjects where selected by convenience from the Faculty of Sports of University of Porto (FADEUP). The participants had no noticeable physical impairments and body height, mass and date of birth were registered for scaling purposes. Seven subjects (age: 25.1 $\pm$ 2.7 yrs; height: 173.1 $\pm$ 9.2 cm; mass: 68.0 $\pm$ 10.0kg) were asked to perform static and gait trials with 26 reflective markers and 7 IMUs consistently placed between subjects. The joint angles during static pose were used to align the differences in the orientation of each segment anatomical frame determined using the IMUs and Qualisys.

Additionally, a preliminary object-based test was conducted using a toy track and a car to evaluate the potential of another IMU engineered at Champalimaud Foundation, named "Wear". Four reflective markers were placed on the top of an Xsens sensor and for comparison means Wear was fixed on Xsens (see Figure 4.5) and both local axis were aligned (manually). Horizontal sliding movements with the IMUs fixed over a toy car were performed to discard gravity, which Qualisys does not account for.

4.1 Optical Motion Capture System

Concurrent validity was assessed in both cases using kinematic data from 12-camera Qualisys (3 Oqus310 plus 9 Oqus400), functioning at a typical frequency of 100Hz. Cameras were placed at 2.0 $\pm$ 0.9m in an arc around an indoor testing in LABIOMEP. A small webcam (HP Webcam HD 2300) was also used to collect the video for each test. Wand calibration was performed as recommended by manufacturer: a rigid wand, with two markers mounted, was moved inside the volume of interest in all three directions to extract camera's relative position and orientation; a L-shaped reference structure was further placed on the ground to determine the lab coordinate system. Figure 4.1 shows the laboratory reference frame with XYZ designation. Y-axis is directed anteriorly, in the direction of the movement, Z-axis points upward vertically and finally X-axis

laterally and orthogonal to the other two axis.

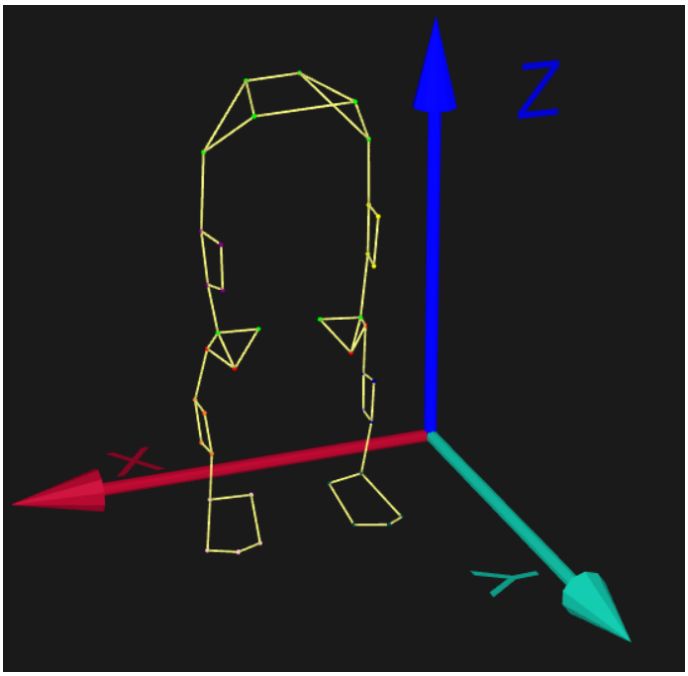

Figure 4.1: Laboratory reference frame. Qualisys Track Manager Screen for lower limbs.

Regarding the subject-based trials, the calibration lasted 60 seconds and was wide and long enough so that the markers didn't lose track during the walking trials. The reconstruction error was consistently below 0.8 mm and the exposure/threshold adjustments were performed with closer markers, simulating fibula head and lateral epicondyle of the femur distance.

In the toy track test the calibration lasted 30 seconds with a reconstruction error of 0.5 mm capturing table volume of interest.

4.2 Inertial Systems

4.2.1 Xsens Inertial Data

Each MTw Awinda sensor (47 x 30 x 13 mm), weights 16g and integrates 3D accelerometer (scale:$\pm$ 160 m/s^2, noise: 0.002 $m/s^2/\sqrt{Hz}$), 3D gyroscope ($\pm$2000 deg/s, 0.01 $deg/s/\sqrt{Hz}$), 3D magnetometer ($\pm$1.9Gauss, 0.2m $Gauss/\sqrt{Hz}$) and a barometer (300-1100 $mBar^{10}$, 0.85 Pa/$\sqrt{Hz}$). With Awinda, the battery can be in operation for up to approximately 6 hours. The data is further transmitted to the Awinda Master (Awinda Station or Awinda USB Dongle). MTw Awinda provides 3D angular velocity using rate micro-electromechanical (MEMS) gyroscopes, 3D linear acceleration using MEMS accelerometers and 3D earth magnetic field using magnetometers. The technical drawing of the sensor was created on Autodesk® Inventor® and is represented in Figure 4.2.

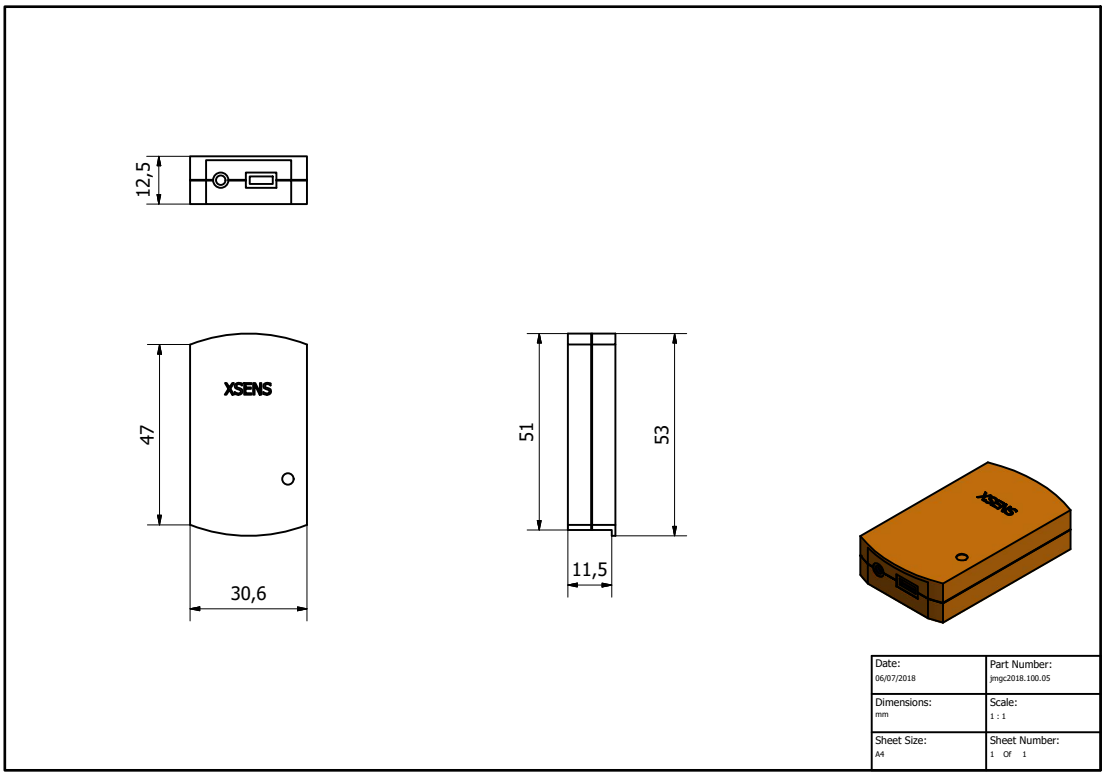

Figure 4.2: Technical drawing of the Xsens MTw Awinda sensor.

Kinetikos Link software allows to communicate directly with Xsens IMUs. Among other features it holds an important property, specially when collecting data with humans - sensors alignment reset. This property makes all sensor's coordinate system align, independently of the segment orientation in which they are attached. This alignment was performed in every trial before subjects performed the asked activity.

In some cases a static trial is used just to record the subject is in static pose, which can be used as a starting reference for subsequent measurements.

4.2.2 Wear Inertial Data

In previous years the Champalimaud's Hardware Platform (Champalimaud Foundation) developed an IMUs system for human research. It is a 9-axis integrated system comprising 3-axis accelerometer, 3-axis gyroscope and 3-axis magnetometer and weights merely 2g. Its small battery lasts up to approximately 4 hours. More dimension details are represented in Figure 4.3, which corresponds to the technical drawing created on Autodesk® Inventor®. This hardware is still under development and was used to assess the potential for greater biomechanical studies comparing its acceleration measurements with Qualisys and Xsens.

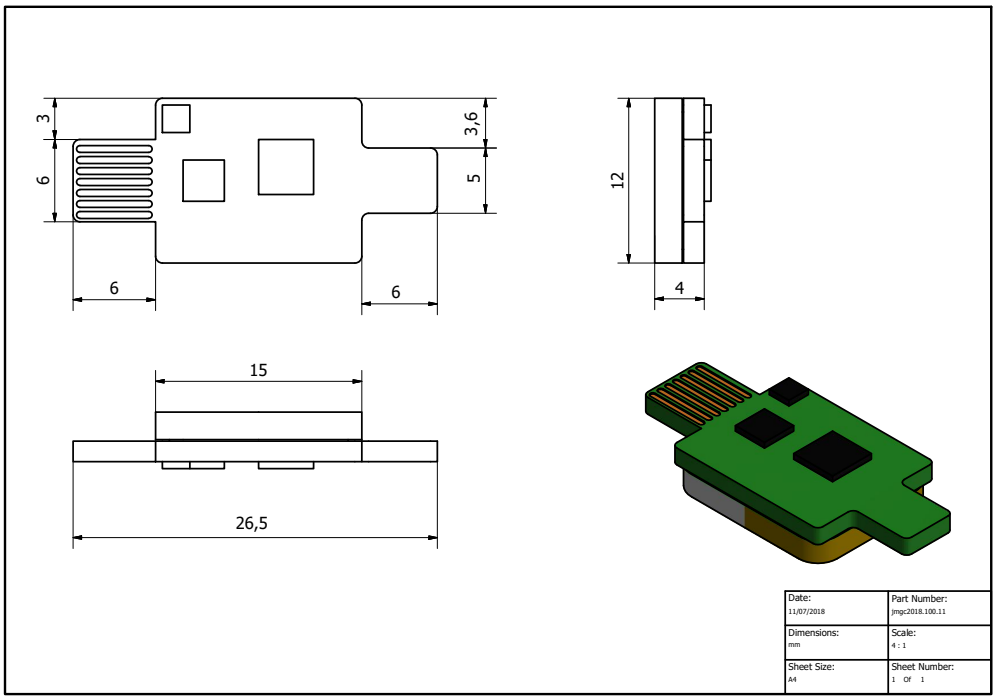

Figure 4.3: Technical drawing of the Wear IMU sensor.

4.3 Experimental setup with subjects

Subject-based studies are intended to depict walking activities concerning the right lower limb joints: hip, knee and ankle. These and other joints are covered by Kinetikos biomechanics models, where in the case of this study, hip internal/external rotation, hip abduction/adduction, hip flexion/extension, knee flexion/extension, and ankle dorsi/plantar flexion were used.

Each subject experiment began with a approximately 20 seconds static recording with the subjects standing in an upright posture, where the Xsens' IMUs were previously reset aligned followed by a gait trial. This step serves as a static calibration to establish the hip, knee and ankle angles offsets.

Kinetikos Link alignment reset, mentioned in section 4.2.1, was performed in two distinct ways: (i) the first one, with subjects No.1 up to subject No.5, this step was performed before Qualisys started recording, which may have left room for possible movements in the meantime, and then, a new recording containing the walking data was collected; (ii) the second way was applied to subject No.6 and subject No.7 and the alignment reset button was hit in Qualisys time, knowing roughly the moment when both systems were perfectly aligned. However, the time counting was made by an independent timer, due to the fact that it was not possible to mark this time in Qualisys records. In this case, immediately after the static part, the subjects started walking until the end of recording.

The static trials are fundamental to scale the kinematic model to the subjects and establish

it's joint angles offsets. The gait trial consisted in five repetitions of self-selected pace, walking around two signaling cones delimiting the walking area.

The inertial and optical systems were collected at 100 Hz and synchronized by an external source emitting a 5V trigger signal. The Xsens received a pulse on the rising edges and Qualisys started in the falling edges of the 5V step signal.

Concerning the IMUs, they were preferably affixed on quadriad and aligned to the axis defined by orthogonal vectors connecting the retro reflective markers or alternatively held with straps. This additional set of cluster markers (see Figure 4.4) adds redundancy in case the markers detach during the trials as explained in Chapter 2.

The markers placement on anatomical landmarks followed International Society of Biomechanics (ISB) recommendations on definitions of joint coordinate systems for the lower limbs joints [58]. Additionally, three markers were placed on the dorsal margin/aspect of the 1^{st}, 2^{nd} and 5^{th} metatarsal head according to Istituto Ortopedico Rizzoli's (IOR) marker set. The complete set of markers is discretized in table 4.1 for the lower limbs.

Table 4.1: Markers dataset for Lower Body.

Right Side	**Left Side**	**Anatomical Reference**
R.ASIS	L.ASIS	Anterior superior iliac spine
R.PSIS	L.PSIS	Posterior superior iliac spine
R.Troc	L.Troc	Greater trochanter
R.Thigh.Front_Upper	L.Thigh.Front_Upper	Laterally and distal [23] positioned with the
R.Thigh.Front_Lower	L.Thigh.Front_Lower	longest principal axis of the marker distribution
R.Thigh.Rear_Lower	L.Thigh.Rear_Lower	oriented toward the relevant anatomical
R.Thigh.Rear_Upper	L.Thigh.Rear_Upper	landmark position [22].
R.Knee.Lat	L.Knee.Lat	Epicondylus femoris lateralis
R.Knee.Med	L.Knee.Med	Epicondylus femoris medialis
R.TT	L.TT	Tibial tuberosity
R.FH	L.FH	Fibula head
R.Shank.Front_Upper	L.Shank.Front_Upper	Laterally and distal [23] positioned with the
R.Shank.Front_Lower	L.Shank.Front_Lower	longest principal axis of the marker distribution
R.Shank.Rear_Lower	L.Shank.Rear_Lower	oriented toward the relevant anatomical
R.Shank.Rear_Upper	L.Shank.Rear_Upper	landmark position [22].
R.Ankle.Lat	L.Ankle.Lat	Tip of the lateral malleolus
R.Ankle.Med	L.Ankle.Med	Tip of the medial malleolus
R.Toe.Lat	L.Toe.Lat	Dorsal margin 5th metatarsal head
R.Toe.Med	L.Toe.Med	Dorsal margin of the 1st metatarsal head
R.FM2	L.FM2	Dorsal aspect of the 2nd metatarsal head

Every subject was equipped with seven IMUs placed on lower limbs and pelvis. The positioning of the sensors on each body segment followed the suggestions by Kinetikos team, as to adapt to their processing steps:

(i) Pelvis: placed vertically with the light pointing down over the top of the sacrum between LPSIS and RPSIS markers.

(ii) Thighs: placed horizontally in the central-third on a marker-cluster with the lights point back on the limbs.

(iii) Shanks: placed horizontally on a marker-cluster with the lights point back on the limbs.

(iv) Feet: placed vertically with a small strap over the flat portion of the feet and with the light pointing up .

It should be noted that the IMUs placement were sligthly different from the ones suggested by Mangia et al. [54], Xsens tutorials and Kinetikos knowledge base guidance.

Concerning the IMUs, they were preferably affixed on a quadriad (or triad) and aligned to the axis defined by orthogonal vectors connecting the retro reflective markers or alternatively held with straps. According to Baré et. al [23] and Cappozo et. al [22] the cluster should be laterally and distal positioned, with the longest principal axis of the marker distribution oriented toward the relevant anatomical landmark position. Figure 4.4 exemplifies one subject with the marker set and IMUs positioned for static and walking trials.

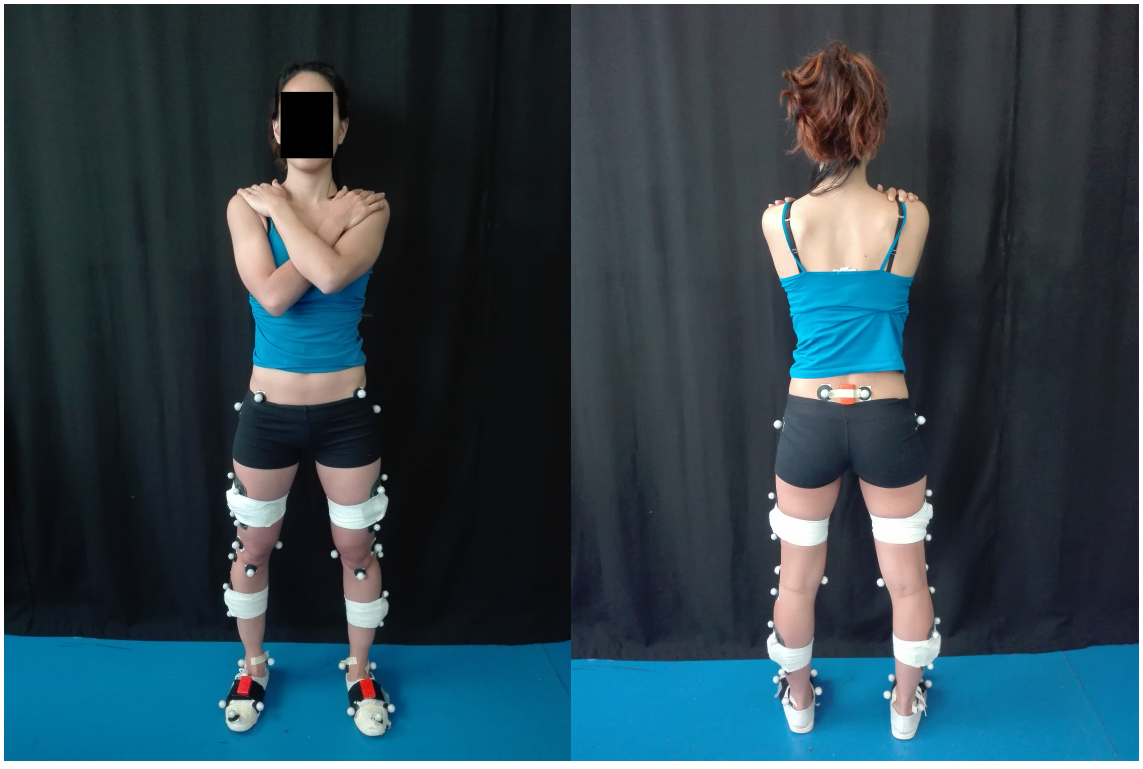

Figure 4.4: Front (left) and back (right) view of subject No.1 with reflective markers and IMUs mounted.

Because IMUs are prone to magnetic disturbances, before proceed with the experiments, it was chosen a "magnetically safe" place with no clipping indication on magnetometer data. Then,

all participants stayed at the very least 2.5 seconds in static position to later warm-up the post processing filter.

4.3.1 Pre-processing

Optical data processing used the acquisition software Qualisys Track Manager, provided by the same company (Qualisys AB, Sweden), and included filling the marker trajectories. The preferred method was the spline-filled method with polynomial interpolation, where gaps were less than 10 frames. Some movements occurred very quickly and the adjustment proved to be more suitable that the one provided by linear interpolation.

IMU data are rotated/posed with Kinetikos kinematic model in static position so that both reconstructions/position estimates started from the same basis. This correction by the standing reference was already proven to be determinant to decrease the results differences [59]. This step is achieved by Kinetikos proprietary algorithm, feeding the files into Kinetikos platform. Of course, it could simply be considered that in the initial moment all variables are zero, but that would be clinically irrelevant. IMU-based or OMC-based data were then translated to achieve the best alignment and to allow the calculus of performance indices and further analysis.

4.3.2 Statistical Analysis

To assess the performance of Xsens MTw Awinda in joint angle measurement under walking conditions, two metrics were calculated for each subject: Mean Absolute Error (MAE), and Pearson's Correlation Coefficient (ρ) also referred to as Pearson's r. The analyses were performed using Matlab®R2017a.

MAE enables the comparison of one measurement technique, the gold standard, against an alternative technique. MAE will measure the average magnitude of the errors in that set of predictions obtained with the alternative approach. Root Mean Squared Error (RMSE) is also a metric to measure accuracy but, as it squares the errors before they are averaged, it increases the relative weight given to occasional disparate errors. In other words, large errors will lie far from RMSE regression line and will be accounted greatly, as they will be distanced from the line of best fit.

On the contrary, MAE averages the errors without considering their direction, and attributes equal weights to each difference between observed and predicted angle value:

$$MAE = \frac{1}{n}\sum_{j=1}^{n} \mid q_{\theta j} - x_{\theta j} \mid, \mid e_{\theta j} \mid = \mid q_{\theta j} - x_{\theta j} \mid, \tag{4.1}$$

where $q\theta j$ is the expected angle value measured with Qualisys and $x\theta j$ is the correspondent prediction calculated with Xsens. The corresponding error is designated by $e\theta j$ and n is the total number of frames used in each trial, correspondent to 10 gait cycles. For each trial, the MAE for each lower limb joint (hip, knee and ankle) was calculated to measure the accuracy of the mean joint angles, estimated with MTw Awinda.

The waveform similarity was assessed using Pearson's *r*, which is a statistical measure that calculates the strength of the relationship between the relative displacements of the inertial and optical-based joint angles. It ranges between -1.0 and 1.0 and is defined by:

$$\rho_{qx} = \frac{Cov(\theta_q, \theta_x)}{\sigma_q \sigma_x} = \frac{E[(Q-\mu_q)(X-\mu_x)]}{\sigma_q \sigma_x,} \tag{4.2}$$

where $\mathrm{Cov}(\theta_q,\theta_x)$ is the covariance matrix, μ_q and μ_x correspond to the expected values for the Qualisys and Xsens angles, respectively. The correspondent standard deviations are σ_q and σ_x and E represents the expected value operator.

A correlation coefficient, between two variables, of 1.0 shows perfect positive similarity, which means that for each positive increase in one variable, the other variable also presents a positive increase, disregarding the magnitude of the increase. On the opposite, -1.0 means perfect negative correlation, when for a positive increase in one variable the other has a negative increase, moving in opposite directions. A correlation of 0.0 means zero or no relationship between the waves shape of the two variables.

4.4 Experimental setup with Object

Wear was fixed on top of Xsens along with four reflective markers of 12 mm. All systems were collected at 100 Hz and synchronized by a 5V trigger signal emitted by Wear station: the Xsens received the pulse on the rising edges and Qualisys started in the falling edges of the 5V step signal (more specifications of the sensors, setup and markers can be found in Appendix 2).

The position and orientation of both Wear and Xsens inertial systems was chosen according with the data visually retrieved from the corresponding software: Bonsai and MT Manager, in this order. The axis documentation from Wear did not correspond with the outputted data and so the orientation provided from its documentations was not considered. The ideal alignment, without any reset in the heading or inclination was found to be the one depicted in Figure 4.5, where both accelerometer and gyroscope data in the three-axis must be aligned. The magnetometer data is not inter-comparable since Wear is overly vulnerable to surrounding magnetic interferences as watches, phones and principally the Xsens where it was attached.

The sliding trial system, represented in Figure 4.6, consisted in a small gutter, fixed over a table, and alternatively aligned with X-axis and Y-axis of Qualisys/Lab coordinate system, where toy car slid over it.

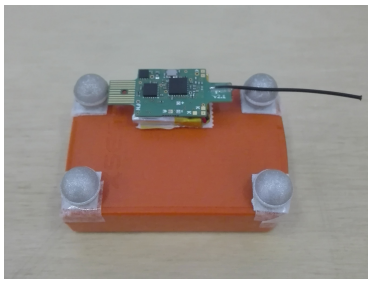

Figure 4.5: Mounting scheme with Wear, Xsens and reflective markers glued on top.

Furthermore, the assembly (Wear plus Xsens plus markers) remained constant, with the axis of the inertial systems, but alternatively aligned with the axis of Qualisys (see Figure 4.7).

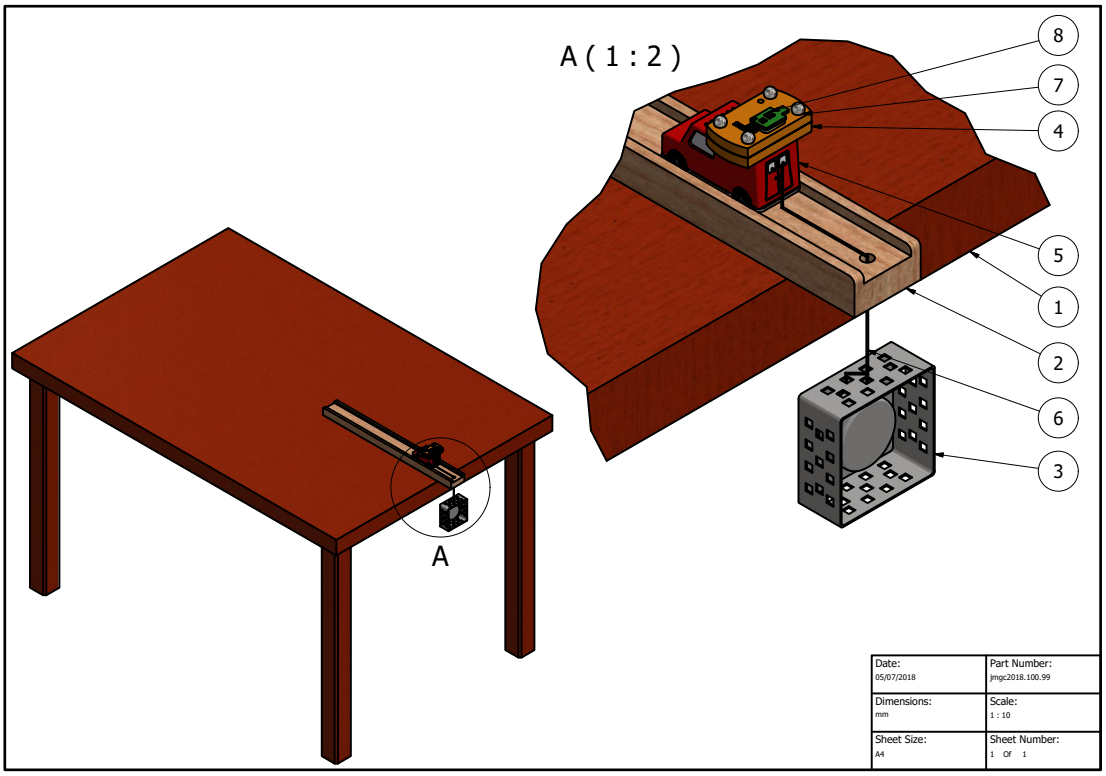

Figure 4.6: Test schematics created on Inventor. Legend: 1-table, 2-track, 3-weight, 4-Xsens, 5-car, 6-wire, 7-reflective marker, 8-Wear.

For example, with the gutter aligned with laboratory Y-axis, the assembly (Wear plus Xsens plus markers), were placed on the car in three distinct positions: with the sensors' X-axis in the direction of laboratory Y-axis, with the sensors' Y-axis in the direction of laboratory Y-axis and finally with the sensors' Z-axis in the direction of laboratory Y-axis. Each assembly-car orientation, depicted in Figure 4.7, was repeated at least three times, making a total of 23 tests.

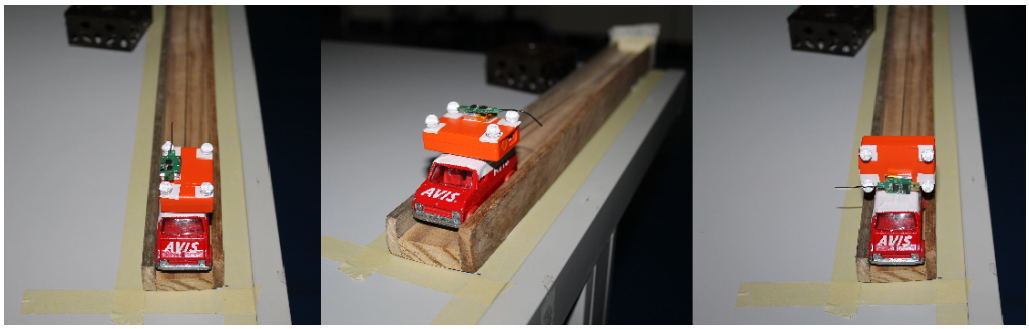

Figure 4.7: Left - Position 1: Sensor's X-axis along the gutter longitudinal axis. Middle - Position 2: Sensor's Y-axis along the gutter longitudinal axis. Right - Position 3: Sensor's Z-axis along the gutter longitudinal axis

4.4.1 Pre-processing and Statistical Analysis

Contrary to the processing in the walking trials, here, the raw data of all three systems were filtered. The first attempt was to evaluate the power spectrum of the accelerometer data, choosing the best cutoff frequency and then, low pass filter it with a 4th order Butterworth. However, the signals spectrum did not allow us to choose the best cutoff frequency for the systems, because it appeared widely scattered over the entire range of permitted frequencies. In the case of the shape of the spectrum being an exponential, or presenting notable peaks, the frequencies of interest would be easily selected however, in this case, it was required another approach, finding a compromise between what was relevant to keep within the signal and the noise to be eliminated. For the purpose, it was tested decreasing frequencies from 49 Hz (Nyquist frequency = 50 Hz) and used as reference a specific aspect of the signals, present is all tests. As soon as the car plus sensors assembly reaches the end of the gutter and the engine stops, the system undergoes a sudden deceleration, corresponding to a strong negative acceleration peak in the signals. As this moment is certain to happen in all the tests, the percentage of decrease of this peak in the filtered signal to the original was the basis for the choice of the cutoff frequency of the filter. A good range of testing would be between 20% and 50%, so that the peak does not disappear and the filtering has some effect, since very low frequencies completely "erase" this peak, and therefore, soften the signal too much, and very high frequencies do not alter it. After testing few cases and observing the results, it was verified that the 30% were the fairer, because above this value the signal suffered too much change compared to the raw data, adulterating the results between the systems.

The offset of the signals was removed as they would start in the same static basis (zero acceleration). Then, the signals were aligned and performance indices were calculated. In most cases the inertial data had to be manually aligned due to the presence of a non-deterministic noise in the data collections. The alignment was attained using the first appearing positive peak right after the assembly starts going through the gutter. The performance indices were calculated between the one hundred frames before the moment of the peak and the peak frame (nearly), as from here, the assembly would be disarranged due to the clash with a barrier, at the end of the gutter, and

it would not make sense to apply any comparison terms. Finally, to evaluate the performance of the systems, the chosen metrics were the MAE (Mean Absolute Error) and ρ (Pearson's Correlation Coefficient), similarly to the gait studies, and the analyses were also performed using Matlab®R2017a.

Chapter 5

Results and Discussion

5.1 Concurrent Validation with subjects

In this chapter are presented the results from the concurrent validation and the preliminary object-based test. The comparisons were obtained through Mean Absolute Error (MAE) and Pearson's Correlation Coefficient (r).

5.1.1 Experimental Results

The motion reconstruction workflow described in 2.3.2 was applied to reconstruct hip, knee and ankle kinematics using data from both Qualisys and Xsens systems.

Additionally, data obtained with Qualisys system were processed using six different combinations of markers' weights (in arbitrary units) to assess the importance of this step in the IK result. For this purpose, we assumed the following reasoning (implemented in Kinetikos software): the parent frame is the pelvis and from there down the tendency in increasing the errors is higher, so the weights given from upper to lower should decrease, since the confidence also decreases. Markers with larger weights mean that IK solver will try more tightly to match the marker's virtual and experimental position, as compared to markers with smaller weights. The weight of a marker will be multiplied by the squared-error term for that marker. And so, markers placed with greater confidence are generally the ones that will have larger weights so as not to increase the error in the least-squares equation 2.6. Table 5.1 presents the values of weights used for each marker and Figure 5.1 the effect on the MAE value.

The resulting joint angles for the lower limbs were compared to those obtained with the inertial sensors while assuming the same model posing.

Table 5.1: Weight of the markers, in arbitrary unit (arb. unit), used in each IK running trial. The shaded lines correspond to the thigh and shank clusters and the bold values the weights that changed from the previous distribution method. The real set of markers is in duplicate for right and left side.

	Weight Distribution Method)					
Markers' Weights (arb. unit)	1	2	3	4	5	6
ASIS	1.0	**10.0**	10.0	**20.0**	20.0	20.0
PSIS	1.0	**10.0**	10.0	**20.0**	20.0	20.0
Thigh.Front_Upper	1.0	**5.0**	**1.0**	1.0	1.0	**5.0**
Thigh.Upper	1.0	**5.0**	**1.0**	1.0	1.0	**5.0**
Thigh.Front	1.0	**5.0**	**1.0**	1.0	1.0	**5.0**
Thigh.Rear	1.0	**5.0**	**1.0**	1.0	1.0	**5.0**
Knee.Lat	1.0	**4.0**	4.0	4.0	4.0	4.0
Knee.Med	1.0	**4.0**	4.0	4.0	4.0	4.0
Shank.Upper	1.0	**4.0**	4.0	4.0	4.0	4.0
Shank.Front	1.0	**4.0**	4.0	4.0	4.0	4.0
Shank.Front_Upper	1.0	**3.0**	**1.0**	1.0	1.0	**3.0**
Shank.Rear	1.0	**3.0**	**1.0**	1.0	1.0	**3.0**
Shank.Rear_Lower	1.0	**3.0**	**1.0**	1.0	1.0	**3.0**
Shank.Front_Lower	1.0	**3.0**	**1.0**	1.0	1.0	**3.0**
Ankle.Lat	1.0	**2.0**	2.0	2.0	**4.0**	**2.0**
Ankle.Med	1.0	**2.0**	2.0	2.0	**4.0**	**2.0**
Midfoot.Lat	1.0	1.0	1.0	1.0	1.0	1.0
Toe.Med	1.0	1.0	1.0	1.0	1.0	1.0
Toe.Tip	1.0	1.0	1.0	1.0	1.0	1.0

The values of the error (MAE) and of the correlation that each weight distribution method scored are reported in Table 5.2. The same amount of static part were preserved between subjects for comparison purposes. This way, eliminating the influence that the static part might have had in the final error.

The graph in Figure 5.1 shows the effect of IK running trial choice in the final error for the lower limb joints. Only the right side were evaluated and the MAE represents the average for the seven participants. Each boxplot in Figure 5.3 shows how the overall error of each lower limb joint evolves along the weight distribution methods.

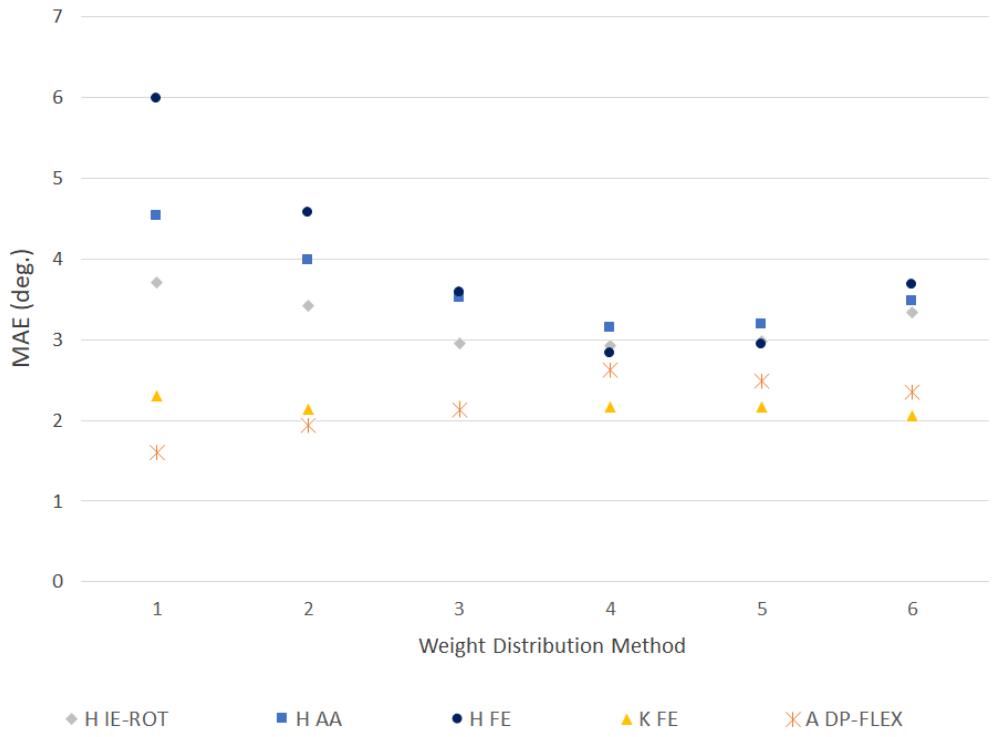

Figure 5.1: Evolution of the MAE in the joints motion reconstruction for the walking trials. The symbols represent the average MAE in each weight distribution method, accounting all participants. H_{IE-ROT}: hip internal/external rotation, H_{AA}: hip abduction/adduction, H_{FE}: hip flexion/extension, K_{FE}: knee flexion/extension, and $A_{DP-FLEX}$: ankle dorsi/plantar flexion.

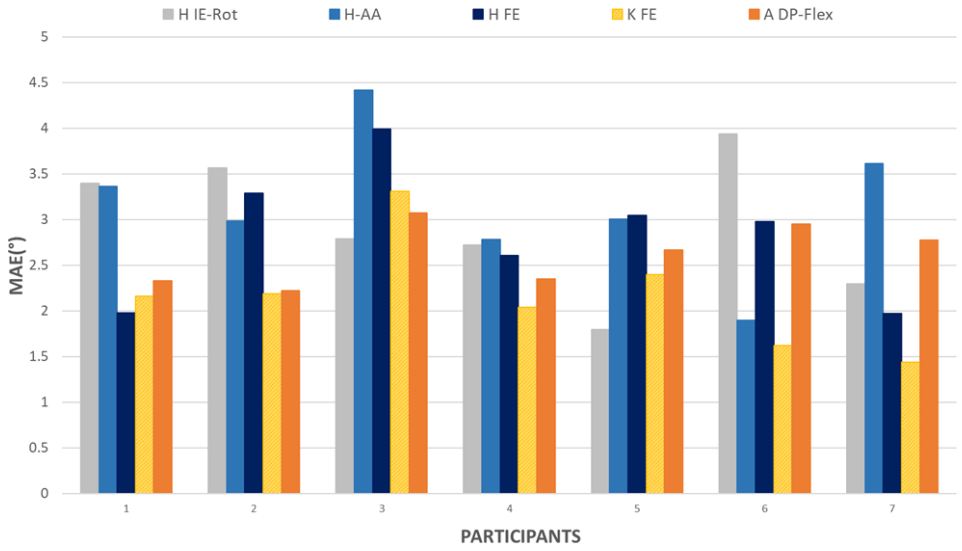

Figure 5.2: Overall MAE results divided by participant.

Table 5.2: Mean absolute error (MAE) and Pearson's Correlation Coefficient (r) estimates using distinct weight distribution methods. MAE and r are calculated according to Equations 4.1 and 4.2 for hip internal/external rotation H_{IE-ROT} , hip abduction/adduction H_{AA} , hip flexion/extension H_{FE}, knee flexion/extension K_{FE} , and ankle dorsi/plantar flexion $A_{DP-FLEX}$. Bold values highlight methods that performed better in MAE.

	H_{IE-ROT}		H_{AA}		H_{FE}		K_{FE}		$A_{DP-FLEX}$		Mean	
Method	MAE	r	MAE	r	MAE	r	MAE	r	MAE	r	MAE	r
1	3.71	0.91	4.54	0.64	5.99	0.95	2.31	0.99	**1.61**	0.96	3.63	0.89
2	3.41	0.92	3.98	0.65	4.58	0.96	2.14	0.99	1.94	0.95	3.21	0.90
3	2.96	0.93	3.51	0.70	3.59	0.97	2.18	0.99	2.13	0.94	2.87	0.91
4	**2.93**	0.94	**3.15**	0.73	**2.84**	0.97	2.17	0.99	2.62	0.93	**2.74**	0.91
5	2.98	0.94	3.18	0.72	2.94	0.97	2.18	0.99	2.49	0.93	**2.75**	0.91
6	3.34	0.93	3.48	0.68	3.68	0.97	**2.06**	0.99	2.36	0.94	2.98	0.90

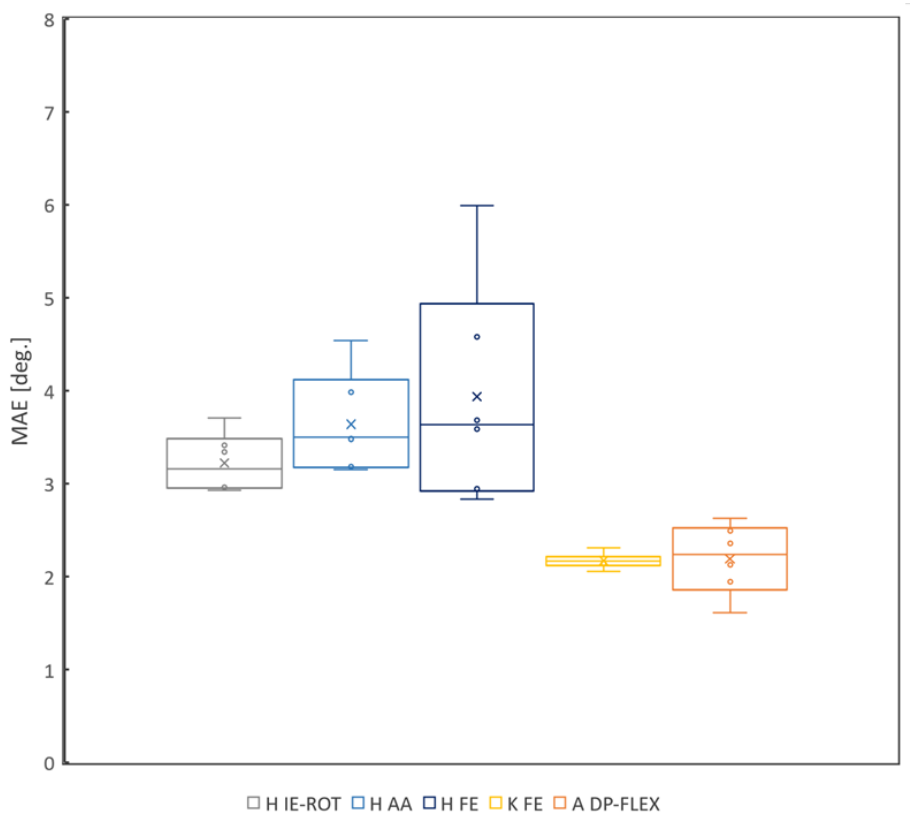

Figure 5.3: Overall MAE results. The central lines correspond to the 2nd quartile (median), Q_2, the upper line the 3rd quartile, Q_3, and the lower line the 1st quartile, Q_1. The whiskers represent the lower and upper limits and the cross symbol the mean MAE. Outlier values lie outside the whiskers.

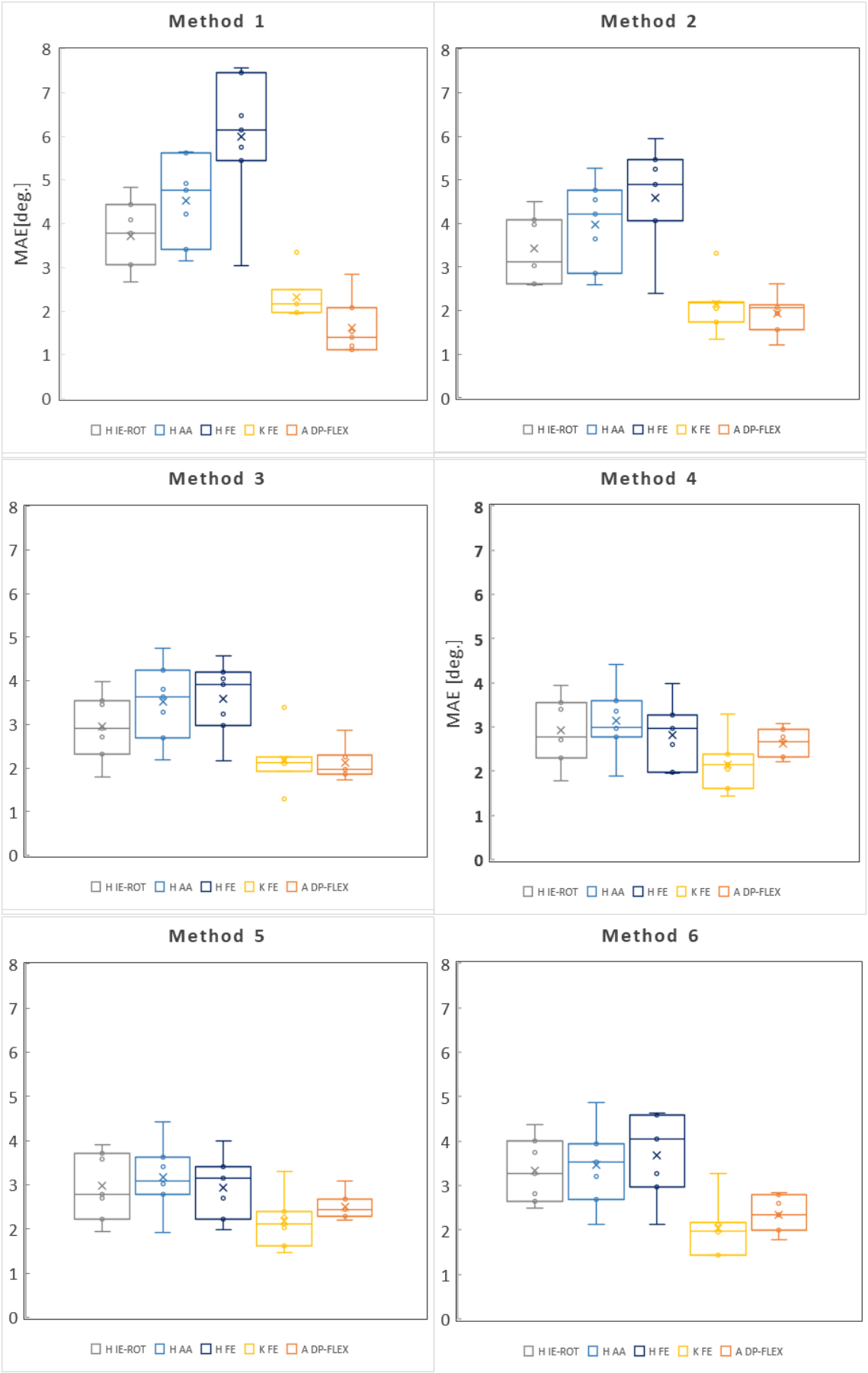

Figure 5.4: MAE results for each tested weight distribution methods. The central lines correspond to the 2nd quartile (median), Q_2, the upper line the 3rd quartile, Q_3 and the lower line the 1st quartile, Q_1. The whiskers represent the lower and upper limits and the cross symbol the mean MAE. Outlier values lie outside the wiskers.

5.1.2 Discussion

IMU-based an OMC-based systems can now be compared through two suggested statistical measures: Mean Absolute Error, MAE, and Pearson's Correlation Coefficient, r.

5.1.2.1 MAE

MAE is commonly used to verify the proximity of expected values to known results and thus, as OMC data were considered the "gold standard" and accordingly the known values, IMU-derive kinematics are the predictions. Therefore, from Table 5.2, we see that the weights combination used in method 4 have lowered the MAE in all hip DoFs, being comparable with method 5. This leads to the conclusion that higher relative weights on pelvis markers plus "discarding" cluster markers generate better results at the hip. In correspondence, the best results for the ankle (1.61° were attained without much effort, using relative weights of 1.0 in all markers (weight distribution method 1). It can be concluded that the ankle tracking is improved when the other markers are not over-weighted relative to that of the ankle/foot. Regarding the weight distribution impact on knee's MAE, the variations were to small to support any kind of interdependence.

Using default weights of 1.0 (arb. unit) for all markers (method 1) the hip errors were quite large, certainly because there was no anatomical points on the trunk to aid the tracking of the pelvis. Therefore, to tightly match the kinematics, the hip markers weights were increased in a systematic manner.

Furthermore, Figure 5.1 and Table 5.2 show that the most problematic joint was the hip in all its degrees of freedom. With weight distribution method 1, in which all the markers equally influenced the kinematics, the hip flexion/extension MAE were 6°, hip adduction/abduction 4.54° and hip internal/external rotation 3.71° of MAE. However, other weights combinations were tested and it was possible to achieve fairly good results at hip flexion/extension in method 4 and method 5 (MAE < 3.2°). This hip DoF is given more importance since most walking dynamics take place in the sagittal plane.

Since what changed from method 1 up to method 6 was mainly the relative weight attributed to the markers placed on the hip: ASIS and PSIS, it can be infer that as we increase the weight of these markers in relation to the others, the hip position estimation with the two systems come drastically closer. On the contrary, the ankle orientation error increases as the hip ones decrease, yet, achieving quite small MAE in all cases with the biggest error of 2.6°. The knee behaviour is the least prone to significant variations, maintaining in all cases errors below 2.3° and, additionally, from Figure 5.3 we see that K_{FE} presents the lowest distance between quartiles (Q_3-Q_1), which sustain the aforementioned interpretation.

Also, from boxplots in Figure 5.3, the global error for H_{FE} is clearly the most affected by changing the markers' weights, followed by H_{AA} and A_{DP}.

Another consistent test across weight distribution methods was to evaluate the influence of the clusters in the inverse kinematics. Comparing methods 2-3 and 6-4, it can be perceived that in either cases, when cluster markers weights decrease to the default 1.0, the H_{FE} MAE decreases

almost 1° but $A_{DP-FLEX}$ tend to slightly increase. This concludes that the clusters have no significant use to improve hip orientation estimation, but have some relevance when comes to tracking ankle joint and a little less relevance for the knee.

We could start distinguishing the methods by qualifying the inter-quartile difference, Q_3-Q_1, and outliers points, since these serve as a measure of data variability, which is desirable to reduce. Thereby, the worst performing methods would be method 1-3, with extreme outliers at knee level joint.

Even so, these outliers have high extreme values and hence, should be discarded from the data series as they may be quietly increasing the MAE in the remaining methods. Through intrinsic observation, it can be concluded that these extreme results probably belong to participant 3 (see Figure 5.2), which are consistently higher than those in other subjects (except for H_{IE-ROT}).

From Figure 5.4 we can see that methods 4 and 5 are the best cases as they present for all DoFs the third quartile below 4° of error. The second quartile (median) in the these methods (methods 4 and 5) does not vary notably, which is proven by the results presented in Table 5.2, where both MAE and r have more or less the same mean values. With a MAE of 2.7° mean, we are within the dynamic error range of Xsens MTx ($\approx 3°RMSE$) [60]. Hence, it was not significant to explore another weights combination because the compensation would be really small or even, unmeasurable. As explained above, it was expected that the last two subjects would lead to better results since the alignment reset occurred on Qualisys time was noted and used to discard the previous marker data. For subject No.7, we can say that the outcome went as expected, since in the DoFs of interest (in the saggital plane) the errors are below 3°, which is the knee best result within the group. Also in Figure 5.2 we see that subject No.1 also presents MAE below 3° in the saggital plane, with better results than subject No.6 at the hip and ankle level. This could be due to some misplacement of hip markers (ASIS or PSIS) in that particular subject, or probably subject No.1 remained really static in the upright posture trial.

For the purpose of this thesis (and also for pedagogical reasons) we opt to manually manipulate markers weights to assess its consequence on IK results. Nevertheless, an automatic and systematic solution could be implemented to automatically search for the best set of weights.

5.1.2.2 Pearson's Correlation Coefficient (r)

The second measure that was studied is Pearson's Correlation Coefficient (r or ρ) and evaluates, within a scale -1.0 and 1.0, how well the IMU-estimated kinematics follow the reconstruction pattern obtained with OMC [61]. If a good r is attained then the signals shape does not vary significantly, which means that a virtual character will act similarly with any of the alternative systems, and the reconstruction will naturally converge.

Comparing with the DoF reflected in the saggital plane, the ankle drosi/plantar flexion achieved the lowest correlation, what can be due to the use of shoes during the walking trials. These results might be improved with subjects walking barefoot with the markers and IMU placed directly on surface skin.

From the perspective of r, Table 5.2 points method 1 as the best to follow A_{DP} pattern, methods 3-6 to track H_{FE} and no significant preference concerning knee joint. Method 4-5 for H_{IE-ROT} and method 4 for H_{AA}.

However, correlation coefficients present propensity to be distorted when in presence of outliers, which may wrongly infer any relationship between the variables. As subject No.3 (see Figure 5.2) may have lead to the outliers visible in Figure 5.4, our discussion will not depend to much on this performance index.

Clusters and isolated skin marker displacements are subject-specific, so they might have non-systematically influenced the results.

5.2 Summary

Generally, considering MAE and r, the best weight distribution method to reconstruct the motion would be method 4, comparable to method 5 with MAE of 2.7° and r of 0.91°. Either methods decreased the first errors in more than 3°, which had really high impact in the final results. Of course there are infinite other combinations of markers weights as a result, a global optimization approach would search for the best combination among all markers weights and subjects what would probably ensure that we had the best results possible. However, the attempts of decreasing the errors were made manually, and since we only tested six solutions, we would have been very lucky to hit the best combination.

It is described that the best performance of IMU-based systems is achieved in the main motion plane [59], which in this case is the saggital plane. This supports this thesis results, where H_{IE-ROT} (transverse plane) and H_{AA} (coronal plane), in fact, present the worst MAE between signals 2.93° and 3.15, respectively, yet they are still great results. On the other hand, the flexion/extension FE angles estimate revealed the highest accuracy (MAE < 2.7°). In general, the kinematic patterns agreed considerably (MAE = 2.74 and r = 0.91) and the overall MAE ranged between 2.2°-3.1°, being that the lowest was K_{FE} and highest the H_{AA}.

To endorse our findings, we have adopted the studies from [10] that are comparable with ours (evaluate the same DoFs) and added some more to Table 6.1 in Appendix **??**. Our findings are comparable to previous works when measuring sagittal ankle, knee and hip joint kinematics during walking that obtained errors of 1.9°-4.8° [61], even though the markers were placed on top of the sensor which discards the SA effect. Also a similar study [62] obtained MAE between 1.2°-4.5°, being that the lowest value were the ankle dorsi/plantar flexion and the highest the hip internal/external rotation, however, it is not described whether or not the subjects used shoes while walking. Later, [63] achieved 2.2°-3.1° using MAV (Mean Absolute Variablity) as similarity indicator. Oddly, its best result was for hip abduction/adduction and the worse at hip internal/external rotation and hip flexion. Here, contrary to our study, the subjects walked wearing only socks, which does might have been relevant to decrease errors in ankle joint kinematics.

An equivalent study, aided by UWB, instead of magnetometers (to remove the drift in the yaw angle estimation), conquered in walking/stair climbing RMSE (root mean squared error) of 1.4°-ankle dorsi/plantar flexion and 3.5°-knee flexion/extension.

Shortly, Kinetikos motion reconstruction workflow allowed for the estimate of lower limb joint angular kinematics in an accurate manner, validating the utility of inertial systems in outside applications. The greatest discrepancies may be certainly due to the misalignment between the anatomical frames of Xsens and Qualisys at the posing step. Since the joint kinematics are obtained by mean of rotation matrices, the differences in the measured joint angles might lie right there. Also the fact that participants performed the trials wearing shoes and the Xsens on the foot was placed over straps might justify the 1.4° of difference compared to the most similar study [62]. Also, the lack of experience in data collection and palpation of anatomical points by the person who did the recordings might have had negative impact in the results. However, this could be also a favorable condition, since it proves that even with small previous knowledge is possible to attain really good results in short time. Overall, our results corroborate that IMU-based human motion reconstruction is an accurate, easy to use and promising technology.

5.3 Concurrent Validation with object

5.3.1 Experimental Results

The mean results in all planes of study for the 23 performed tests are presented in Table 5.3. However, in some cases the inertial systems failed badly or suffered sampling mismatches (see Figure 5.5), which is why it is also presented the results considering only the successful cases in Table 5.4. So, without the failures remained, 18 tests, which continues to be a quite reasonable sample.

Table 5.3: Mean absolute error (MAE) in m/s^2 and Pearson's Correlation Coefficient (r) estimates among 23 sliding trials, pondering success and failure cases.

Qualisys(Q)	Inertial Systems (MT andW)	MAE(m/s^2)			*r*		
		QvsMT	QvsW	MTvsW	QvsMT	QvsW	MTvsW
Y	X	1.10	2.36	2.79	0.79	0.46	0.22
	Y	0.46	1.28	1.23	0.97	0.87	0.83
	Z	0.96	1.29	1.34	0.92	0.70	0.64
X	X	0.78	1.08	1.05	0.91	0.84	0.79
	Y	0.53	0.87	0.71	0.96	0.92	0.92
	Z	0.60	0.95	0.23	0.99	0.81	0.99
Mean		0.74	1.30	1.22	0.92	0.77	0.73

Table 5.4: Mean absolute error (MAE) in m/s^2 and Pearson's Correlation Coefficient (r) estimates among 18 sliding trials discarding the failure cases.

Qualisys(Q)	Inertial Systems (MT andW)	MAE(m/s^2)			*r*		
		QvsMT	QvsW	MTvsW	QvsMT	QvsW	MTvsW
Y	X	0.72	1.03	-	0.98	0.92	-
	Y	0.46	1.28	1.23	0.97	0.87	0.83
	Z	0.93	0.75	0.66	0.94	0.96	0.95
X	X	0.74	0.90	0.96	0.92	0.92	0.87
	Y	0.53	0.87	0.71	0.96	0.92	0.92
	Z	0.60	0.65	0.23	0.99	0.98	0.99
Mean		0.66	0.91	0.76	0.96	0.93	0.91

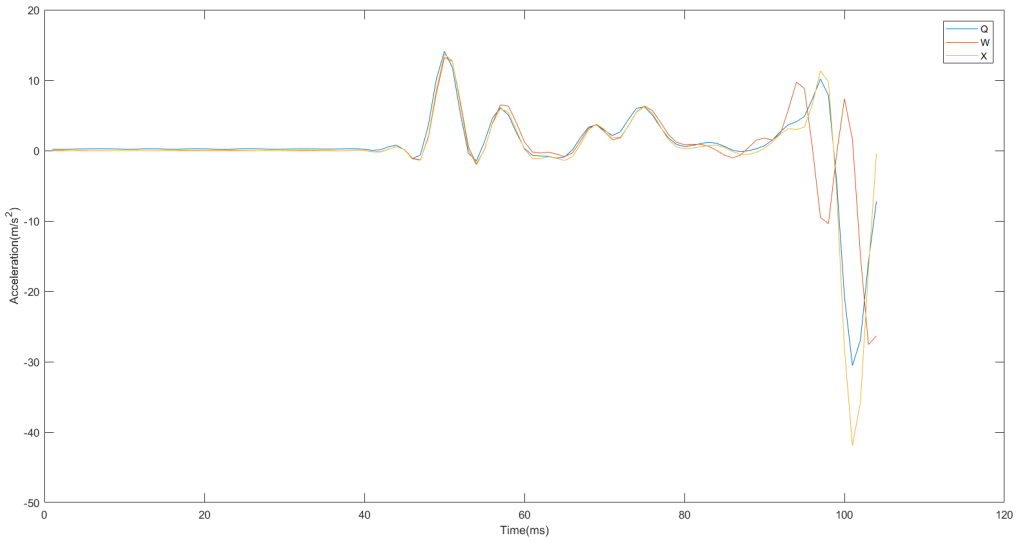

Figure 5.5: Acceleration(m/s^2) vs time (ms) graph showing Wear advance and oscillating waves during the sliding. Q (blue line) stands for Qualisys, W (red line) to Wear and X (orange line) represents Xsens values.

5.3.2 Discussion

The tables above aim to speculate about Wear IMU being a promising method for later biomechanical studies. In 23 tests, the number of success trials decreases 22% to 18 cases. The losses represent the failures in the inertial systems and delays or advances in the Wear inertial unit. In the successful cases the MAE were equal or below 0.91 m/s^2 and r above 0.91. The rudimentary character of the study does not allow us to obtain reproducibility in the results. The wire that was not in constant tension and the slide was not controlled by any initial brake. The spring effect

of the wire prevent the acceleration wave to have the expected shape of a perfect step response, presenting some oscillating waves (see Figure 5.5).

These Wear delays / advances appear to result from high oscillations in the sampling frequency. This should vary between 100 ± 1 (99 and 101), however, by examining the raw files the number of samples in each second varies more than that, sometimes being 98, 103, 105 others 107. An oscillating acquisition frequency between 98 and 107 ($\pm$ 9Hz $\approx$ 10%) is a critical mismatch, which by analysis of the signals the explanation of these delays or advances would then be the gain or loss of samples by the Wear inertial unit.

In both cases, the acceleration errors are higher than expected as compared with [64], which is a robot based motion where the non deterministic noise is greatly decreased. This brings us good expectations when applying these systems to human movement, much less controlled. Nonetheless, for the purpose of obtaining the biomechanical angles, the accelerations needed to be integrated into position, further increasing the present errors.

As future work, less rudimentary tests with greater mechanical control should be performed in order to eliminate the non-deterministic noise and to obtain a step acceleration waveform. For instance, a brake would control the beginning of the slide and ensure that the rope is always taut, and the force being applied would be constant, and as so the acceleration (F=ma). To solve for the Wear issues, data would be collected at higher frequencies followed by down sampling to same amount of samples per second.

Chapter 6

Conclusions and Future Work

The main goal of this thesis was to conduct a concurrent validity study, using a motion reconstruct system (Kinetikos, Coimbra, Portugal), where the MTw Awinda (Xsens Technologies B.V., Enschede, the Netherlands), was compared against the "gold standard" camera optical motion capture system (Qualisys AB, Sweden). Based on this study results we can conclude that by combining Kinetikos physics-based models of human biomechanics with measurements of movement from body worn inertial sensors we can accurately reconstruct human motion matching the results of an OMC system.

This is only possible when the same biomechanical model is applied and both calculus start from the same basis. So, besides the offset between correspondent angles measured by MAE, was also evaluated if the pattern of the calculated angles follows the same variation through correlation coefficient. As so, the final errors might be justified by the mismatches between the human subject and the computer model. Yet, adding another system with intrinsic dynamic accuracy of approximately 3° (Xsens) naturally increases the associated error. The errors are smaller and the correlation rates higher when the range of motion is wider, i.e. in the saggital plane. For future work, we stress the need to run similar experiments in other free daily living activities (involving both lower and upper limbs) and clinical relevant populations.

6.1 Obstacles

Generally, our results are comparable to those reported in literature, sometimes better and other times worse but in the same order of magnitude. Many issues can be considered to explain our results:

i Synchronization problems of the 3 kinematic systems (two inertial and one optical). The functioning of the trigger did not always work, and whenever the voltage was below 5V the optical system was not triggered;

ii Lack of experience in data collection and palpation of anatomical points by the person who did the recordings. This could be also a favorable condition, since it proves that even with small previous knowledge is possible to attain really good results in short time;

iii Readjustments in the collection procedures. Testing different ways to when reset align Xsens IMUs in order to obtain a feasible posing;

iv Posing of the models without knowing the exact time at which the two kinematic systems were in the same basis;

v Preprocessing of walking data. We did not consider filtering neither optical data or inertial one. This could eventually decrease the errors, however by graphs visualization the difference would not be significant;

vi An optimization approach was not created in order to go trough all participants and all weights combinations. It would have an overly demanding programming component that was not the focus for this thesis.

vii The rudimentary character of the preliminary study introduces non-deterministic errors to the system, which probably prevented more promising results.

6.2 Goals Satisfaction and Future Work

Although IMUs have been widely used in instrumented movement analysis to aid clinical assessment, rehabilitation, sports, diagnostics, etc., there are still some gaps that need to be explored.

Several studies on sit to stand movement and gait analysis obtained promising results supporting the idea of inertial alternatives. However, comparative studies involving the upper limbs are not so straightforward, as the light reflected or emitted by the markers during the movement might be obstructed, preventing their visibility by the cameras. An incoming work, would be to study upper limbs' kinematics, which is predicted to be more challenging due to the lower range of successful experiments that cover this body part and the associated shoulder complexity.

Also, the validity of IMUs was reported to be speed-specific [12] and task-specific and [65], which would be a great point testing faster movements, like running or kicking a ball in the future. Finally, we were able to support the idea and further prove that a lower complexity system with smaller cost and size is capable of accurately estimate the target orientation and position of a body, kicking in biomechanics' guidelines. Regarding the preliminary test, greater mechanical control should be applied in order to eliminate the non-deterministic noise and obtain as expected a step acceleration waveform. Furthermore, similarly gait trials using Wear units and Qualisys would certificate the hardware and eventually lead to more complex studies such as scapular movements.

Appendix

Appendix 1. Gather of lower limbs methods presented here and in [10].

Table 6.1: Summary of Concurrent Validation studies targeting Lower Limbs kinematics.

Ref.	Year	Sensors	Kinematics and constraints	Sensor Fusion approach	Validation	Measure	Error	C	Comments
[62]	2008	2 acc, 2 gyro , 2 mag	-	-	OMC	hip rot hip ad hip fle knee fle ankle fle	4.5 3.6 3 2.4 1.2	-	one gait cycle, walk MAE
[61]	2013	-	-	-	OMC	hip rot hip ad hip fle knee fle ankle fle	3.0 4.8 2.5 1.9 2.1	0.96 0.39 0.99 0.99 0.99	markers on imus top one gait cycle, walk , MAE, CMC
[63]	2014	7 acc	rot mat	TRIAD like	OMC	hip rot hip ad hip fle knee fle ankle fle	3.1 2.2 3.1 3.0 2.6	0.90 0.96 0.99 0.97 0.92	walk, right side. MAV, r
[66]	2016	7acc, 7gyro, 3 UWB	kinematic chain, rot mat	KF	OMC	hip ad hip fle knee fle ankle fle	2.9 2.7 3.5 1.4	- - - -	100s walk/ stairs climbing RMSE
Our	2018	7 acc, 7 gyro, 7mag	kinematic chain	KF	OMC	hip rot hip ad hip fle knee fle ankle fle	2.9 3.1 2.8 2.2 2.6	0.94 0.73 0.97 0.99 0.93	30s walk MAE, r

Table 6.2: List of abbreviations.

Abbreviation	**Full Name**
acc	accelerometer
gyro	gyroscope
mag	magnetometer
UWB	ultra wide band
int	integration
rot mat	rotation matrix
KF	Kalman Filter
OMC	Optical Motion Capture
ad	abduction/adduction
rot	rotation
fle	flexion/extension
MAE	Mean Absolute Error
MAV	Mean Absolute Variability
RMSE	Root Mean Squared Error
CC	Coefficient of Correlation
CMC	Coefficient of Multiple Correlation
r	Pearson's Correlation Coefficient

Appendix 2. Preliminary test specifications

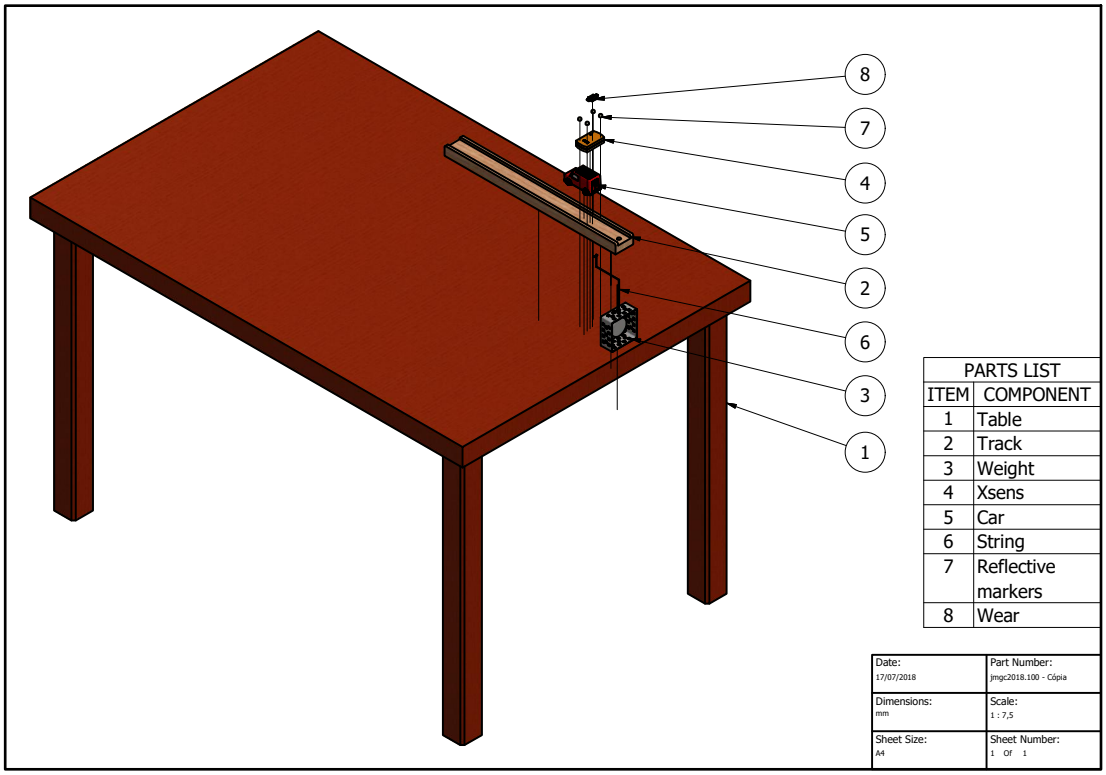

Figure 6.1: Exploded view of all experimental set up.

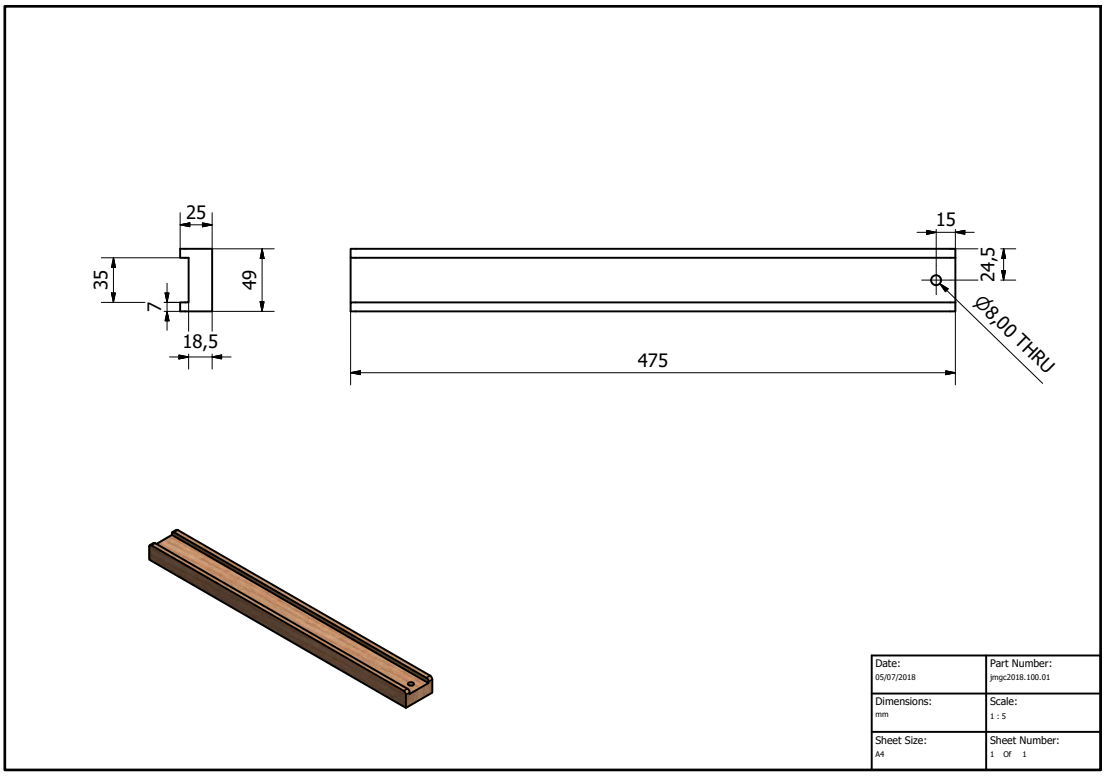

Figure 6.2: Track specifications.

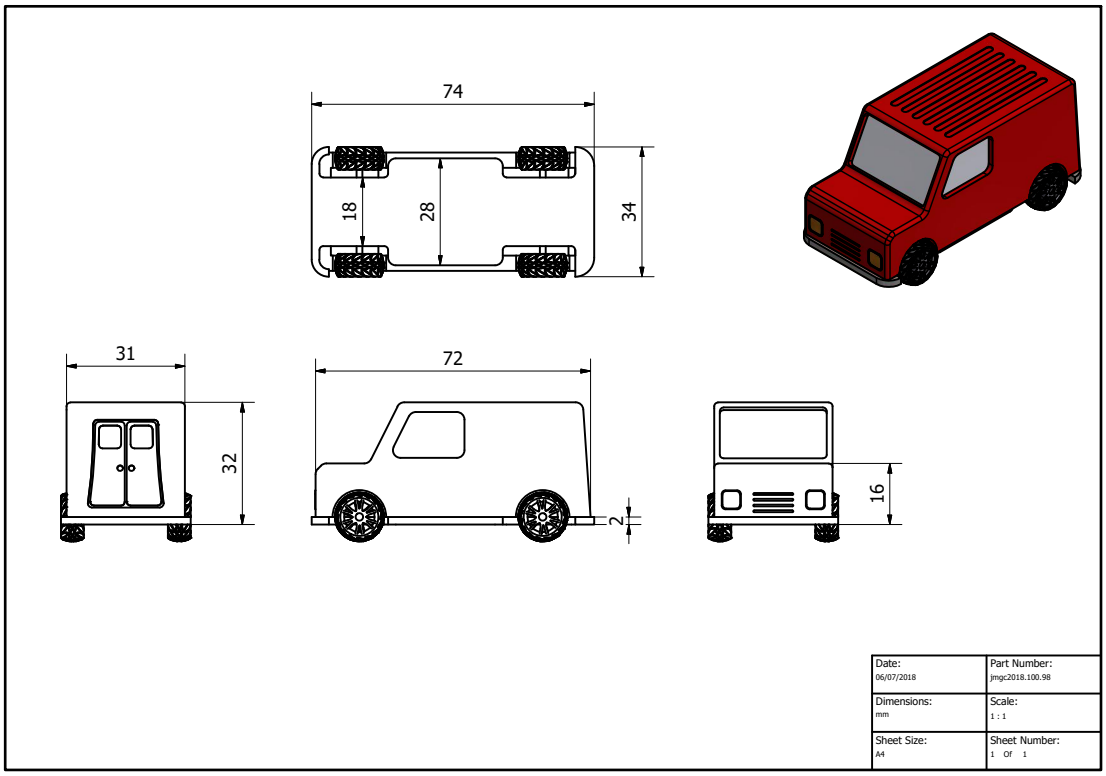

Figure 6.3: Car specifications.

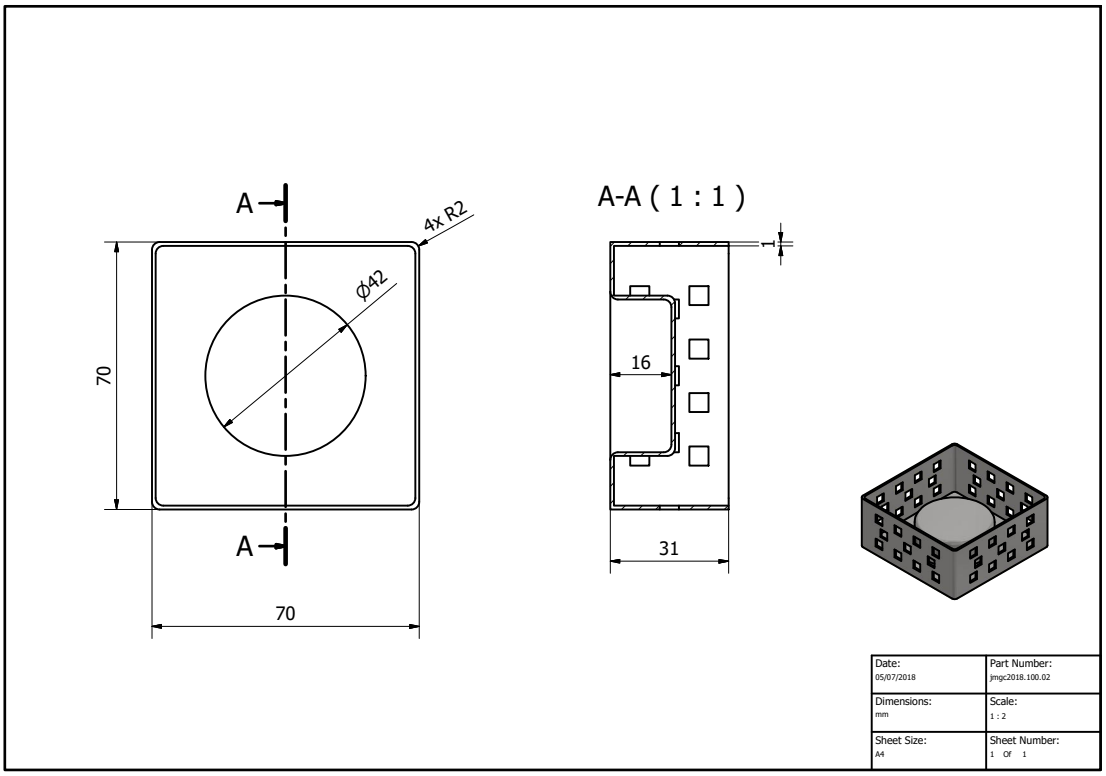

Figure 6.4: Weight specifications.

References

[1] Omar Salah, Ahmed A Ramadan, Salvatore Sessa, Ahmed M R Fath El-bab, Ahmed Aboismail, Yo Kobayashi, A Takanishi, and M Fujie. Sit to Stand Sensing Using Wearable IMUs Based on Adaptive Neuro Fuzzy and Kalman Filter . pages 288–291, 2014.

[2] Biomechanics | definition of biomechanics by Medical dictionary. URL: `https://medical-dictionary.thefreedictionary.com/biomechanics(Accessed:2018-01-26)`.

[3] Polhemus History - Over 40 Years of Experience. URL: `https://polhemus.com/company/history/(Accessed:2018-07-03)`.

[4] Thomas B. Moeslund and Erik Granum. A survey of computer vision-based human motion capture. *Comput. Vis. Image Underst.*, 81(3):231–268, 2001.

[5] Maria Carmo Vilas-Boas and Paulo Silva Cunha. Movement Quantification in Neurological Diseases : Methods and Applications. 9:15–31, 2016.

[6] Sarah R Fletcher, Teegan L Johnson, and John Thrower. A Study to Trial the Use of Inertial Non-Optical Motion Capture for Ergonomic Analysis of Manufacturing Work. *Part B J. Eng. Manuf.*, 232(1):90–98, 2018.

[7] Amanda L. Martori, Stephanie L. Carey, Redwan Alqasemi, Daniel Ashley, and Rajiv V. Dubey. Characterizing Suitability of Wearable Sensors for Movement Analysis Using a Programmed Robotic Motion. In *Volume 3B: Biomedical and Biotechnology Engineering*, page V03BT03A011. ASME, nov 2013.

[8] Minh H. Pham, Morad Elshehabi, Linda Haertner, Silvia Del Din, Karin Srulijes, Tanja Heger, Matthis Synofzik, Markus A. Hobert, Gert S. Faber, Clint Hansen, Dina Salkovic, Joaquim J. Ferreira, Daniela Berg, álvaro Sanchez-Ferro, Jaap H. van Dieën, Clemens Becker, Lynn Rochester, Gerhard Schmidt, and Walter Maetzler. Validation of a step detection algorithm during straight walking and turning in Patients with Parkinson's disease and older adults using an inertial measurement unit at the lower back. *Front. Neurol.*, 8(SEP):1–9, 2017.

[9] Giulio Zizzo and Lei Ren. Position Tracking During Human Walking Using an Integrated Wearable Sensing System. *Sensors*, 17(12):2866, 2017.

[10] Alessandro Filippeschi, Norbert Schmitz, Markus Miezal, Gabriele Bleser, Emanuele Ruffaldi, and Didier Stricker. Survey of Motion Tracking Methods Based on Inertial Sensors: A Focus on Upper Limb Human Motion. *Sensors*, 17(6):1257, 2017.

[11] Carmen M.N. Brigante, Nunzio Abbate, Adriano Basile, Alessandro Carmelo Faulisi, and Salvatore Sessa. Towards miniaturization of a MEMS-based wearable motion capture system. *IEEE Trans. Ind. Electron.*, 58(8):3234–3241, 2011.

[12] Stephanie Blair, Grant Duthie, Sam Robertson, William Hopkins, and Kevin Ball. Concurrent validation of an inertial measurement system to quantify kicking biomechanics in four football codes. *J. Biomech.*, 2018.

[13] Xsens Technologies B.V. Enschede The Netherlands. Xsens MVN Road Tour Timeline. URL: https://www.xsens.com/customer-cases/?pf=xsens-mvn-analyze(Accessed:2018-01-29).

[14] Xsens Technologies B.V. Enschede The Netherlands. Xsens mvn analyze hardware awinda and link. URL: https://www.xsens.com/products/xsens-mvn-analyze/(Accessed:2018-02-02).

[15] Xsens Technologies B.V. Enschede The Netherlands. Customer cases - xsens 3d motion tracking. URL: https://www.xsens.com/customer-cases/(Accessed:2018-07-23).

[16] Xsens Technologies B.V. Enschede The Netherlands. Study of effects of intent recognition errors on neural control of powered lower limb prostheses - customer cases - xsens 3d motion tracking. URL: https://www.xsens.com/customer-cases/study-effects-intent-recognition-errors-neural-control-powered-lower-limb-prosth(Accessed:2018-07-23).

[17] Metria Innovation, Inc |, N Street, and Milwaukee. 3D Motion Capture Buyer's Guide Motion Capture System Description Major Brands Major Components Advantages Disadvantages. (414):763–2426. URL: http://www.metriainnovation.com/userdata/userfiles/file/Metria-BuyersGuide-v1.pdf.

[18] Manon Kok, Jeroen D Hol, and Thomas B Schön. Using Inertial Sensors for Position and Orientation Estimation. 2017.

[19] Bikramjit Basu. Introduction to Biomechanics and Orthopedic Device Testing. pages 385–407. Springer, Singapore, 2017.

[20] D Gordon E Robertson, Graham E Caldwell, and Joseph Hamill. *Research Methods in Biomechanics, Second Edition*. 2004.

[21] a Cappozzo, F Catani, U Della Croce, and a Leardini. Position and orietnation in space of bones during movement. *Clin. Biomech.*, 10(4):171–178, 1995.

[22] Aurelio Cappozzo, Angelo Cappello, Ugo Delia Croce, and Francesco Pensalfini. Surface-marker cluster design criteria for 3-d bone movement reconstruction. *IEEE Trans. Biomed. Eng.*, 44(12):1165–1174, 1997.

[23] Arnaud Barré, Brigitte M. Jolles, Nicolas Theumann, and Kamiar Aminian. Soft tissue artifact distribution on lower limbs during treadmill gait: Influence of skin markers' location on cluster design. *J. Biomech.*, 48(10):1965–1971, 2015.

[24] Lin Yang, Shiwei Ye, Zhibo Wang, Zhipei Huang, Jiankang Wu, Yongmei Kong, and Li Zhang. An error-based micro-sensor capture system for real-time motion estimation. *Journal of Semiconductors*, 38(10):105004, oct 2017.

[25] V. Sholukha, B. Bonnechere, P. Salvia, F. Moiseev, M. Rooze, and S. Van Sint Jan. Model-based approach for human kinematics reconstruction from markerless and marker-based motion analysis systems. *Journal of Biomechanics*, 46(14):2363 – 2371, 2013.

[26] OpenSim Models - OpenSim Documentation. URL: https://simtk-confluence.stanford.edu/display/OpenSim/OpenSim+Models.

[27] Katherine Elicerio. One position estimation from skin marker co - ordinates using global optimisation with joint constraints. 32:129–134, 2012.

[28] Ajay Seth, Ricardo Matias, António P. Veloso, and Scott L. Delp. A biomechanical model of the scapulothoracic joint to accurately capture scapular kinematics during shoulder movements. *PLoS One*, 11(1):1–18, 2016.

[29] Ajay Seth, Michael Sherman, Peter Eastman, and Scott Delp. Minimal formulation of joint motion for biomechanisms. *Nonlinear Dyn.*, 62(1-2):291–303, 2010.

[30] Di Frühwirth Martin, Di Hirschberg Urs, Sa; Institute for Architecture Zedlacher Stefan, and Austria; Media [IAM], TU-Graz. FORMOTIONS. 2011.

[31] Optical Tracking Markers | PS-tech. URL: http://www.ps-tech.com/optical-trackers/accessories/optical-tracking-markers(Accessed:2018-01-26).

[32] Xsens Technologies B.V. Enschede The Nether-lands. Xsens video tutorials - body measurements. URL: https://tutorial.xsens.com/(Accessed:2018-02-04).

[33] Hans Kainz, Christopher P Carty, Luca Modenese, Roslyn N Boyd, and David G Lloyd. Clinical Biomechanics Estimation of the hip joint centre in human motion analysis : A systematic review. *JCLB*, 30(4):319–329, 2015.

[34] Kaitlin M Jackson, Tyson A C Beach, and David M Andrews. The Effect of an Isometric Hip Muscle Strength Training Protocol on Valgus Angle During a Drop Vertical Jump in Competitive Female Volleyball Players.

[35] Aden Seaman and John McPhee. Comparison of optical and inertial tracking of full golf swings. *Procedia Engineering*, 34:461–466, 2012.

[36] Peter Hinch. Micropyhton madgwick sensor fusion algorithm. URL: https://github.com/micropython-IMU/micropython-fusion/blob/master/README.md#51-heading-pitch-and-roll(Accessed:2018-02-02).

[37] Jung Keun Lee, Edward J Park, and Stephen N Robinovitch. Estimation of Attitude and External Acceleration Using Inertial Sensor Measurement During Various Dynamic Conditions.

[38] M El-Gohary and J McNames. Shoulder and elbow joint angle tracking with inertial sensors. *IEEE Trans. Biomed. Eng.*, 59(9):2635–2641, 2012.

[39] Marco Iosa, Pietro Picerno, Stefano Paolucci, and Giovanni Morone. Wearable inertial sensors for human movement analysis. *Expert Rev. Med. Devices*, 13(7):641–659, 2016.

[40] Ayman El-fatatry. Inertial Measurement Units IMU. *Rto-En-Avt-105*, (October 2002):1–109, 2003.

[41] Sathish K Sankarpandi, Alice J Baldwin, Jaydip Ray, and Claudia Mazzà. Reliability of inertial sensors in the assessment of patients with vestibular disorders: a feasibility study. *BMC Ear. Nose. Throat Disord.*, 17:1, 2017.

[42] F A Magalhães, A Giovanardi, M Cortesi, G Gatta, and S Fantozzi. Three-dimensional kinematic analysis of shoulder through wearable inertial and magnetic sensors during swimming strokes simulation. *XXIV Congr. Int. Soc. Biomech.*, (November 2015), 2013.

[43] Myo | GUI without the G: Going Beyond the Screen with the Myo™ Armband. URL: http://developerblog.myo.com/gui-without-g-going-beyond-screen-myotm-armband/(Accessed: 2018-01-29).

[44] Omar Salah, Ahmed A. Ramadan, Salvatore Sessa, Ahmed Abo Ismail, Makasatsu Fujie, and Atsuo Takanishi. ANFIS-based sensor fusion system of sit-to-stand for elderly people assistive device protocols. *Int. J. Autom. Comput.*, 10(5):405–413, 2013.

[45] Vincent Bonnet, Claudia Mazza, Philippe Fraisse, and Aurelio Cappozzo. Real-time estimate of body kinematics during a planar squat task using a single inertial measurement unit. *IEEE Transactions on Biomedical Engineering*, 60(7):1920–1926, 2013.

[46] Christopher W.G. Phillips, Alexander I.J. Forrester, Dominic A. Hudson, and Stephen R. Turnock. Comparison of Kinematic Acquisition Methods for Musculoskeletal Analysis of Underwater Flykick. *Procedia Engineering*, 72:56–61, 2014.

[47] Mahmoud El-gohary, Lars Holmstrom, Jessie Huisinga, Edward King, James Mcnames, and Fay Horak. Upper Limb Joint Angle Tracking with Inertial Sensors. pages 5629–5632, 2011.

[48] Agnes Zijlstra, Martina Mancini, Ulrich Lindemann, Lorenzo Chiari, and Wiebren Zijlstra. Sit-stand and stand-sit transitions in older adults and patients with Parkinson's disease: Event detection based on motion sensors versus force plates. *J. Neuroeng. Rehabil.*, 9(1):1–10, 2012.

[49] Aleš Janota, Vojtech Šimák, Dušan Nemec, and Jozef Hrbček. Improving the precision and speed of Euler angles computation from low-cost rotation sensor data. *Sensors (Switzerland)*, 15(3):7016–7039, 2015.

[50] OlliW's Bastelseiten » IMU Data Fusing: Complementary, Kalman, and Mahony Filter. URL: http://www.olliw.eu/2013/imu-data-fusing/(Accessed: 2018-02-03).

[51] S.O.H. Madgwick. An efficient orientation filter for inertial and inertial/magnetic sensor arrays. *Rep. x-io Univ.*, page 32, 2010.

[52] MVN Analyze & Animate - Xsens 3D motion tracking. URL: https://www.xsens.com/mvn-studio-pro/(Accessed:2018-02-02).

[53] S. O. H. Madgwick, A. J. L. Harrison, and R. Vaidyanathan. Estimation of IMU and MARG orientation using a gradient descent algorithm. In *2011 IEEE Int. Conf. Rehabil. Robot.*, pages 1–7. IEEE, jun 2011.

[54] Anna Lisa Mangia, Matteo Cortesi, Silvia Fantozzi, Andrea Giovanardi, Davide Borra, and Giorgio Gatta. The use of IMMUs in a water environment: Instrument validation and application of 3D multi-body kinematic analysis in medicine and sport. *Sensors (Switzerland)*, 17(4), 2017.

[55] Marian Blachuta, Rafal Grygiel, Roman Czyba, and Grzegorz Szafranski. Attitude and heading reference system based on 3D complementary filter. In *2014 19th Int. Conf. Methods Model. Autom. Robot.*, pages 851–856. IEEE, sep 2014.

[56] Fakhri Alam, Zhou Zhaihe, and Hu Jiajia. A Comparative Analysis of Orientation Estimation Filters using MEMS based IMU. *2nd Int. Conf. Res. Sci. Eng. Technol.*, pages 86–91, 2014.

[57] Ramsey Faragher. IEEE SIGNAL PROCESSING MAGAZINE [128] Understanding the Basis of the Kalman Filter Via a Simple and Intuitive Derivation. 2012.

[58] Ge Wu, Sorin Siegler, Paul Allard, Chris Kirtley, Alberto Leardini, Dieter Rosenbaum, Mike Whittle, Darryl D D'Lima, Luca Cristofolini, Hartmut Witte, Oskar Schmid, and Ian Stokes. ISB recommendation on definitions of joint coordinate system of various joints for the reporting of human joint motion—part I: ankle, hip, and spine. *J. Biomech.*, 35(4):543–548, 2002.

[59] Marion Mundt, Anna Wisser, Sina David, Thomas Dupré, Valentin Quack, Franz Bamer, Markus Tingart, Wolfgang Potthast, and Bernd Markert. the Influence of Motion Tasks on the Accuracy of Kinematic Motion Patterns of an Imu-Based Measurement System. *35th Conf. Int. Soc. Biomech. Sport.*, pages 817–820, 2017.

[60] Karina Lebel, Patrick Boissy, Mathieu Hamel, and Christian Duval. Inertial measures of motion for clinical biomechanics: Comparative assessment of accuracy under controlled conditions - Changes in accuracy over time. *PLoS One*, 10(3):1–12, 2015.

[61] Jun-Tian Zhang, Alison C Novak, Brenda Brouwer, and Qingguo Li. Concurrent validation of Xsens MVN measurement of lower limb joint angular kinematics. *Physiol. Meas.*, 34(8):N63–N69, aug 2013.

[62] Pietro Picerno, Andrea Cereatti, and Aurelio Cappozzo. Joint kinematics estimate using wearable inertial and magnetic sensing modules. *Gait Posture*, 28(4):588–595, nov 2008.

[63] Eduardo Palermo, Stefano Rossi, Francesca Marini, Fabrizio Patanè, and Paolo Cappa. Experimental evaluation of accuracy and repeatability of a novel body-to-sensor calibration procedure for inertial sensor-based gait analysis. *Measurement: Journal of the International Measurement Confederation*, 52(1):145–155, 6 2014.

[64] Krzysztof Kozlowski. *Robot Motion and Control 2011*. Springer-Verlag London, 2012.

[65] Y. Blache, R. Dumas, A. Lundberg, and M. Begon. Main component of soft tissue artifact of the upper-limbs with respect to different functional, daily life and sports movements. *J. Biomech.*, 62:39–46, 2017.

[66] Shaghayegh Zihajehzadeh and Edward J. Park. A novel biomechanical model-aided imu/uwb fusion for magnetometer-free lower body motion capture. *IEEE Transactions on Systems, Man, and Cybernetics: Systems*, 47:927–938, 2017.